

## **Appendix B: Supplemental Analysis Confirmation**

# **Seismic Study - Final Report**

## **Washington Monument, National Park Service**

July 31, 2012



**NAMA 184461 WAMO Seismic**  
**NPS Contract: C2000080100**  
**NPS Task Order: P12PD20437**

## **Seismic Study - Final Report Washington Monument, National Park Service**



---

**Mike Korolyk, SE**  
**Evaluator, TM**



---

**Leo Panian, SE**  
**Reviewer, TM**

**Prepared for:**

**National Park Service  
Denver Service Center - Contracting Service Division  
12795 W. Alameda Parkway  
Lakewood, CO 80228**

**Prepared by:**

**Tipping Mar  
Structural Engineering  
1906 Shattuck Avenue  
Berkeley, CA 94704**

## 1 Summary

The purpose of the evaluation is to identify potential vulnerabilities of the Washington Monument under seismic excitations and to make retrofit recommendations as warranted. This study was performed to verify and supplement the analysis performed and recommendations made by Wiss, Janney, Elstner Associates, Inc. (WJE). The evaluation includes consideration of two site-specific seismic hazards developed by the geotechnical engineering consultant, *AMEC Environment & Infrastructure*. The recommendations are intended to achieve the *Basic Safety Objective* (BSO), as defined by ASCE 41-06, *Seismic Rehabilitation of Existing Buildings*.

The evaluation was conducted using a nonlinear analytical model of the monument to represent all of the components that would significantly affect its dynamic behavior during an earthquake. The critical material parameters of masonry stiffness and friction between courses of masonry were varied, creating multiple permutations of the model, considering upper and lower bound properties. Thus, the resulting range of behavior encompasses the effect of uncertainties in material properties. The model was subjected to various recorded ground motions that had been scaled by *AMEC* to represent the type of shaking that might occur at the monument under two different seismic hazards. The first hazard is a benchmark representing the earthquake that occurred in Mineral, Virginia in August 2011. The second hazard represents the Maximum Considered Earthquake (MCE). The response of the structure, with respect to lateral displacement and elemental damage, was reviewed to verify correspondence with observed behavior under the Mineral hazard. The performance assessment was then made considering the MCE.

During the Mineral earthquake in 2011, a significant amount of damage occurred in the upper-most part of the monument (the *pyramidion*). This damage included cracks in some face panel stones, lateral offsets between some face panel stones and their supporting ribs, and broken supports where the panels rest upon the ribs. The observed damage is similar of that predicted by the analysis results for ground shaking representing this earthquake.

The results of the MCE analysis predict damage in the pyramidion similar to what occurred during the Mineral event. It appears unlikely that an MCE would cause significantly more damage than the Mineral earthquake. The predicted damage under the MCE does not indicate that stability of the monument nor of the pyramidion in particular is at risk. However, there is some risk from falling hazards, particularly due to the vulnerability of some of the connections between the panels and supporting ribs.

Under MCE shaking, the analysis indicates that inelastic transient lateral deformations, between one-half inches and one inch, could occur in the upper half of the tower between the 300-foot and 470-foot levels of the monument, depending on the permutation of the model. Corresponding residual lateral deformations are predicted to be between zero and one-half inches. Given that monument walls vary in thickness in these locations between 2'-1" and 8'-6" thick, and that the tower varies in plan width between 48 feet and 34 feet, these deformations are small relative to the thickness of the walls and size of the tower. Global stability of the monument would not be at risk if such deformations did occur.

Under the Mineral shaking the analysis indicates similar damage, but to a lesser degree occurring only near the top of the monument. All inelastic deformations occur above the 350-foot level. Peak inelastic transient and residual lateral deformations are between zero and 3/8 inches, depending on the permutations of the model. After the earthquake that occurred in 2011, residual lateral deformations were observed in which the joints between stones in the same course of masonry widened. The lateral deformations indicated by the analysis may represent the aggregate widening of several such joints.

Based on these findings, seismic improvements are recommended in the pyramidion to reduce the risk from falling hazards. Plans have been developed by *WJE* for repair of the damage caused by the Mineral earthquake. They observed a general correlation of damage to ribs supporting two adjoining face panels. Cracking occurred at the connection between the rib and panel; this condition seems to be more susceptible to damage than cases where the panel runs continuously across the rib. In accord with *WJE*'s recommendations, we recommend expanding the current scope of work to strengthen connections of the same type that experienced cracking during the Mineral event. This work would augment the plans to repair connections already damaged and would entail installing additional brackets and anchor hardware similar to those that are currently part of the repair plans.

## 2 Monument geometry

A significant amount of documentation about the monument exists, so only a cursory description is provided here. This discussion draws primarily from the evaluation report by Oehrlein and Associates Architects, 1993. This report refers to many other historical sources and summarizes how the monument is constructed.

The monument was constructed in two phases. The first phase began in 1848, but construction was stopped in 1854 due to lack of funds. During this phase, the bottom 160 feet of the monument was built upon a foundation that went 23'-4" below grade. The original foundation was underpinned and augmented in 1878 when construction of the monument resumed. Currently, the elevation of the bottom of the foundation is 36'-10" below grade. In plan, it is about 126'-10" square.

Above grade, the lowest 160 feet of the tower comprises of walls roughly 15'-0" thick with cut stone along the interior and exterior faces, and rubble stone in between. The outer dimension of the tower at the base is about 55'-1½" square. Above 160 feet the walls are built entirely of cut stone without the rubble infill. The thickness transitions sharply to about 8'-7" and tapers smoothly to about 1'-6" at 500 feet above grade, about ¼" per foot. The dimension at the base of the pyramidion is about 34'-6".

At roughly the 470-foot level, stone arches (also called ribs) are built integrally with the walls. There are three sets of arches parallel to each orthogonal direction to support the sloped faces of the pyramidion, which begin at the 500-foot level. The sloped pyramidion shell is made of 7" thick stone.

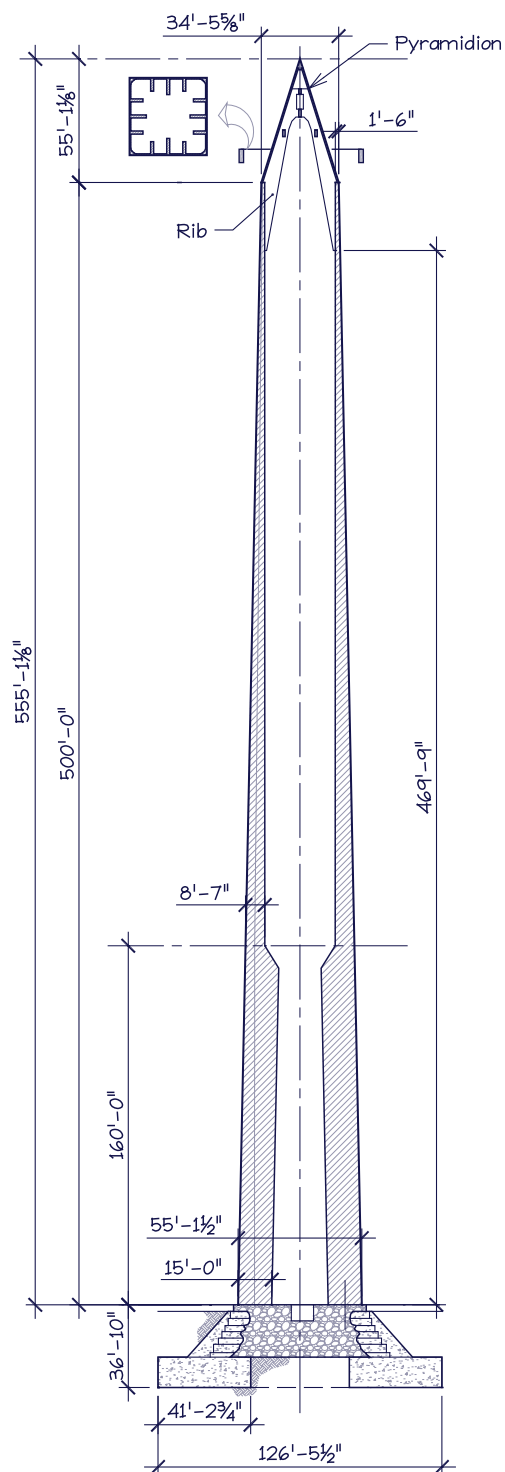


Figure 2-1 Tower section; stairs and elevator omitted.

### **3 Modeling overview**

The computer model was built in three dimensions to capture any effects of horizontal seismic input occurring along two orthogonal directions simultaneously. The nodal locations are typically defined at the geometrical centroid of the elements modeled. The structure is modeled from the base of the footing to the top of the pyramidion. While it is predicted that most nonlinear behavior occurs in the pyramidion, the lower part of the monument is also modeled with nonlinear potential. Below about 470 feet, which is the spring-line of the ribs that form the pyramidion, the tower is meshed into wall elements roughly 8 feet tall and 7 to 10 feet wide. At the boundary between two rows of wall elements is a row of frictional slider elements, to emulate potential sliding planes between courses of masonry. The outside face of the tower tapers by about 8" over 40 feet, but the inside face is not tapered. Following the centroid, each wall element is tilted by about 4" over 40 feet. (Figure 3-1).

Above the 470-foot level, the walls, pyramidion ribs, and face panels are modeled in detail considering the intricate configuration of the ribs that support the sloping face panels. In the pyramidion, the ribs are typically modeled with one discrete wall element per stone, with slider elements placed about every three courses of stone (see section 9).

The foundation has a significantly larger footprint than the base of the tower. It is assumed that any inelastic action that could occur near the foundation would be in the soil or in the tower, but not in the foundation itself, given the size of the foundation relative to the tower at the base and given the strength of the foundation relative to the soil below. Therefore, the foundation is modeled elastically and supported by vertical bar elements assigned compression-only soil material with nonlinear potential. Horizontal restraint is provided at grade and at the base of the footing by stiff elastic bar elements. The validity of this assumption was confirmed by the analysis results.

There is a framework of steel columns and beams inside the tower supporting the stairs and elevator. This construction is not modeled because its stiffness is insignificant in comparison to the masonry. Thus, it is believed the internal stairs, landings, and elevator structures will have no impact on the dynamic behavior of the structure.

The software selected for modeling is Perform 3D by Computers and Structures, Inc. (version 5, released June 2011). This software has an extensive library of components that make it a powerful tool for nonlinear response history analysis. Its primary focus is analysis of structures under seismic loading. The component library allows one to enter a variety of nonlinear force-deformation relationships at the elemental level. These relationships are not overly burdened with complicated options in behavior, facilitating simpler input and the ability to bound complicated behavior using parametric studies. This platform provides a suitable basis for the purposes of this effort to draw broad conclusions about the necessity and nature of possible seismic improvements.

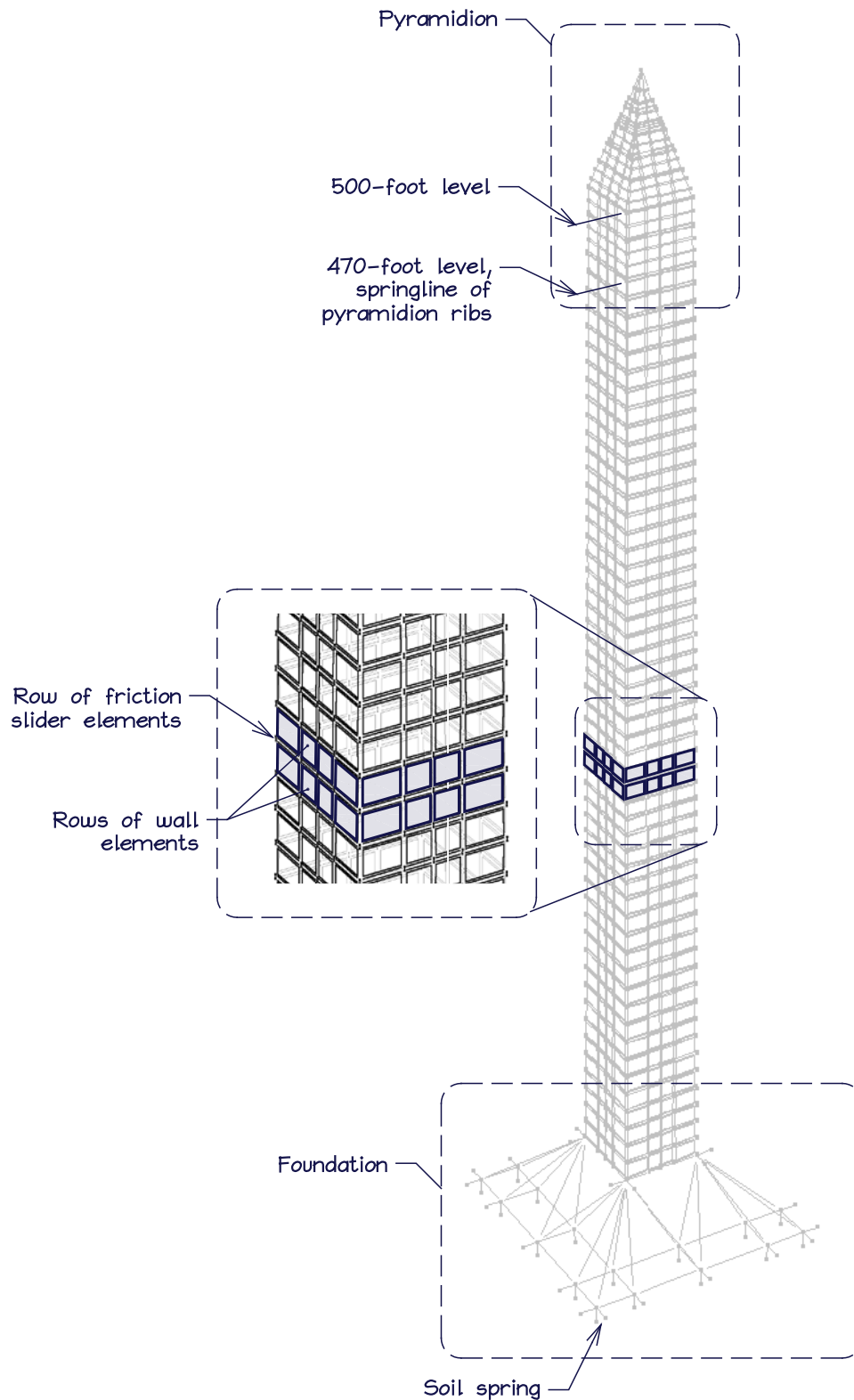


Figure 3-1 Isometric view of the model.

## **4 Materials**

Components in the model such as bars, fiber cross-sections, and walls are defined with a material reference and corresponding area. These materials are defined by a stress-strain relationship defining a backbone curve that envelopes the hysteresis loop of the given material. Aspects of the hysteresis loops vary depending on the type of material selected. The following subsections describe the materials used in the model.

### **4.1 Stone masonry**

Stone masonry material is used throughout the model in the wall elements. This material is of the type *Inelastic 1D Concrete Material*, which defines its hysteretic behavior. It has the following features (see Figure 4-2):

1. Nominal tension capacity,
2. Unloading stiffness equal to initial stiffness,
3. Reloading stiffness computed based on previous maximum strain.

The bottom 160 feet of the monument is constructed of a composite of cut stone at the faces and rubble in between, and above the walls are entirely of cut stone. The stone/rubble composite material properties are computed using a weighted average of the stone and rubble properties assuming the cross-section is proportioned with 30% stone and 70% rubble based on the cross-section of the monument shown in Figure 4-1. Given the heterogeneity of the material, it is likely to dissipate energy cycling at small deformations. This may affect the dynamic behavior of this particular structure in which there are very few sources of energy dissipation and damping. Thus, the material is assigned a relatively low "yield" stress (FY in Figure 4-2) beyond which a small amount of hysteretic damping will occur.

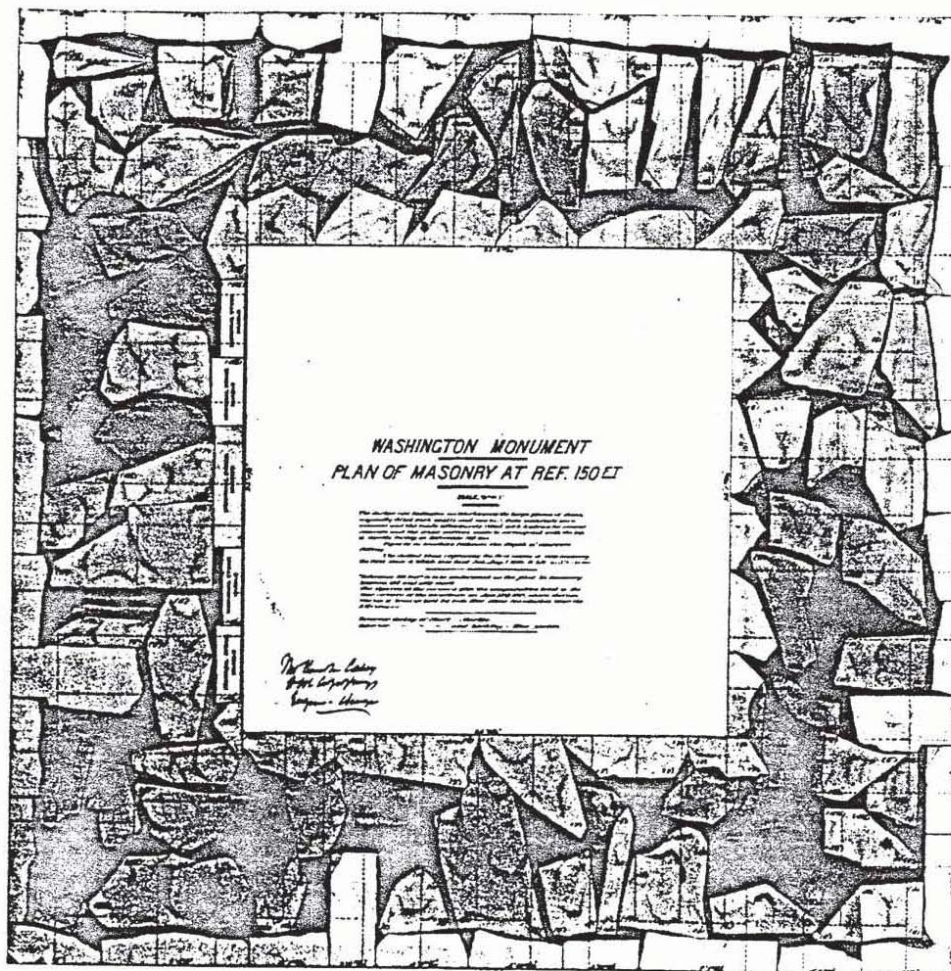


Figure 4-1 Section of tower at the 150-foot elevation, excerpted from Figure 3 of the evaluation report by Oehrlein and Associates Architects, 1993).

The actual mechanical properties of the masonry in situ are not known precisely, and the range of possible properties is wide. Further, stiffness and strength can vary for stone quarried from the same location, and workmanship during placement can affect the properties of the masonry and thus the dynamic behavior of the monument during an earthquake. Given uncertainty of the material properties and likely variability within the monument, parallel analyses were conducted using assumptions to bound the mechanical properties and resulting behavior. Base values for masonry stiffness consistent with those used by *WJE* are tabulated in Table 4-1.

Table 4-1 Base values for masonry stiffness, ksi.

	Below 150 feet	150 feet-470 feet	470 feet-500 feet	Pyramidion
E	1,000	2,000	1,000	5,700

The bounding assumptions represent a range of roughly 0.8 to 2.0 times the base stiffness values. Similarly, the strength of the masonry in compression is bounded as indicated in Figure 4-2.

Models were also created to bound the possible range of tensile capacity. A base value of 100 psi was assumed, for which the results are reported in detail in section 13. Analyses were run assuming a reduced tensile stress capacity of 20 psi, and selected results are reported for comparison in section 14.

This bounding approach entails building multiple models, each being identical with the exception of the material model of interest. A similar approach is used to model frictional sliding actions (see section 5.4).

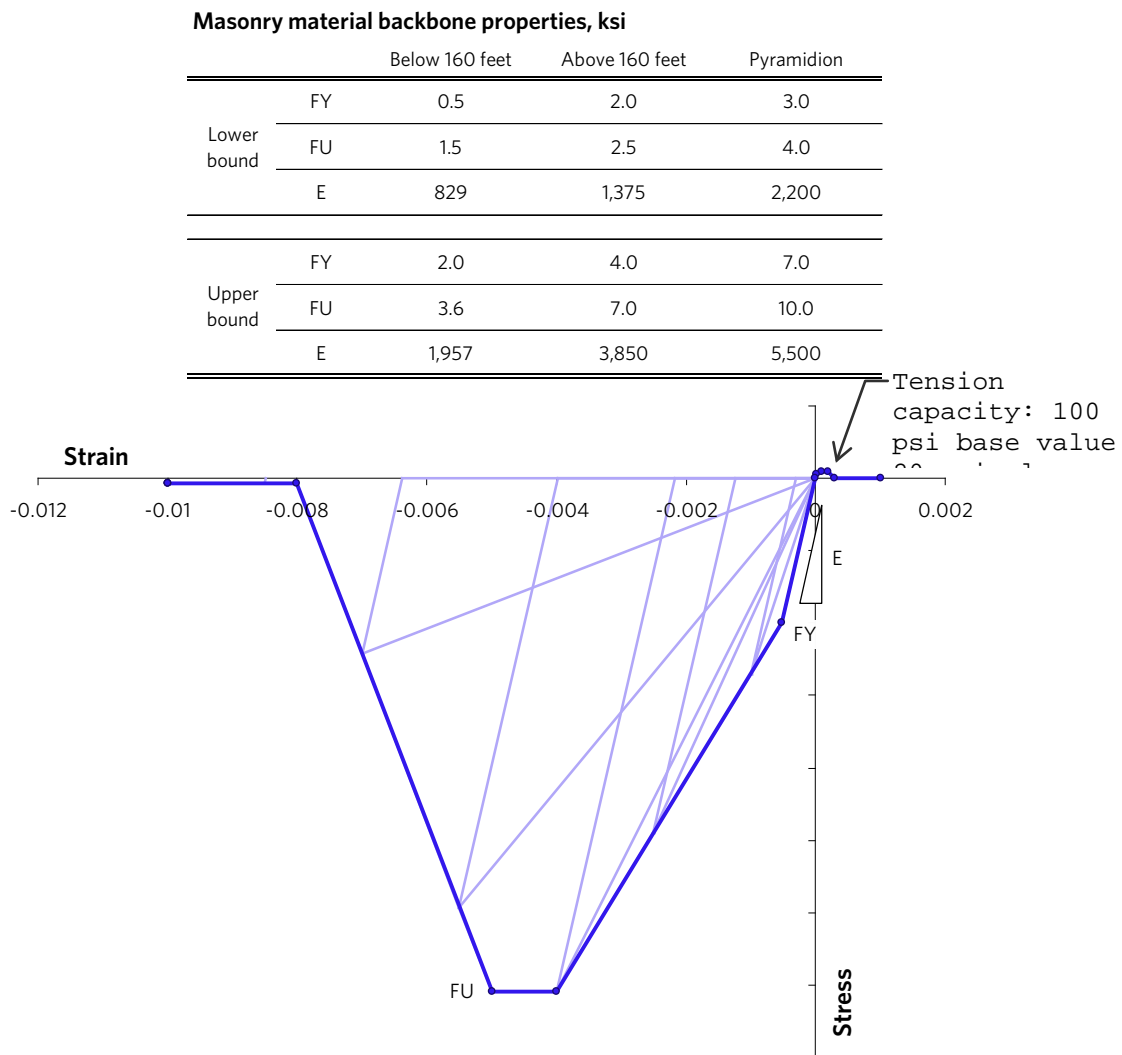


Figure 4-2 Graph of stone material backbone and hysteresis.

## 4.2 Soil

The geotechnical engineers *AMEC Environment & Infrastructure* have provided a load-deformation relationship for the soil. This relationship is nonlinear even for very small deformations (on the order of 0.5 inches) yet is defined to a deflection of 30 inches. The soil material backbone curve in the model focuses on the range of deformation demands expected in the model based on preliminary analyses: less than 2 inches (Figure 4-3). An elastic stiffness is chosen equal to the first stiffness of the soil load deformation curve from *AMEC*, and a yield stress of 4 ksf. The stress is set at a deflection of 1.5 inches so that the area of the load-deformation curve from and *AMEC* and the linearized version of it in the model integrate to zero as shown in Figure 4-4. The hysteresis of this material, bounded by the linearized backbone curve, is plotted in Figure 4-5.

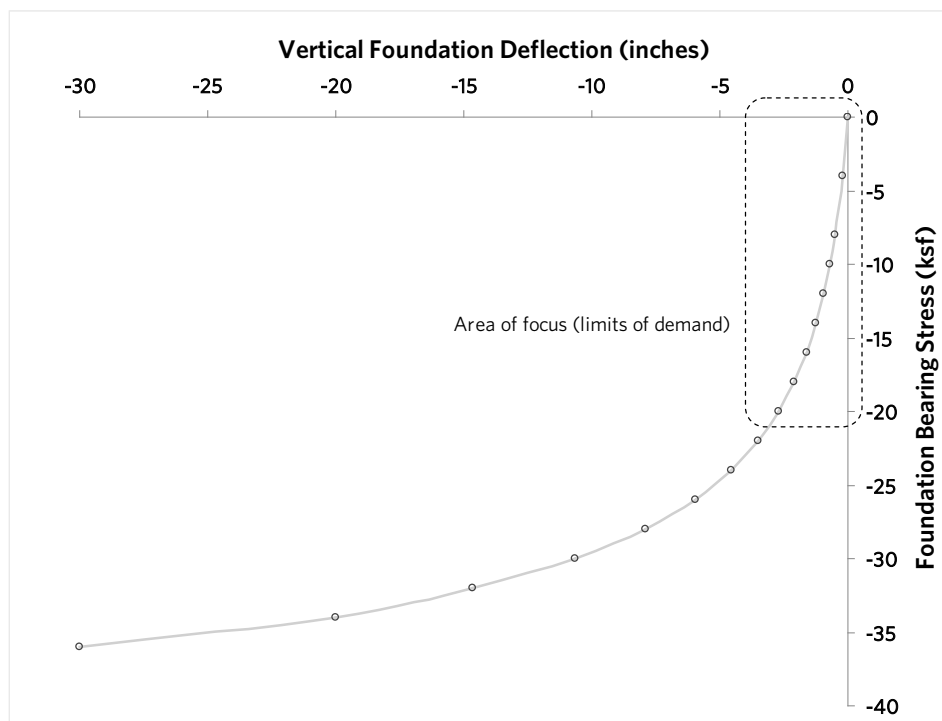


Figure 4-3 Graph of full soil material backbone from AMEC.

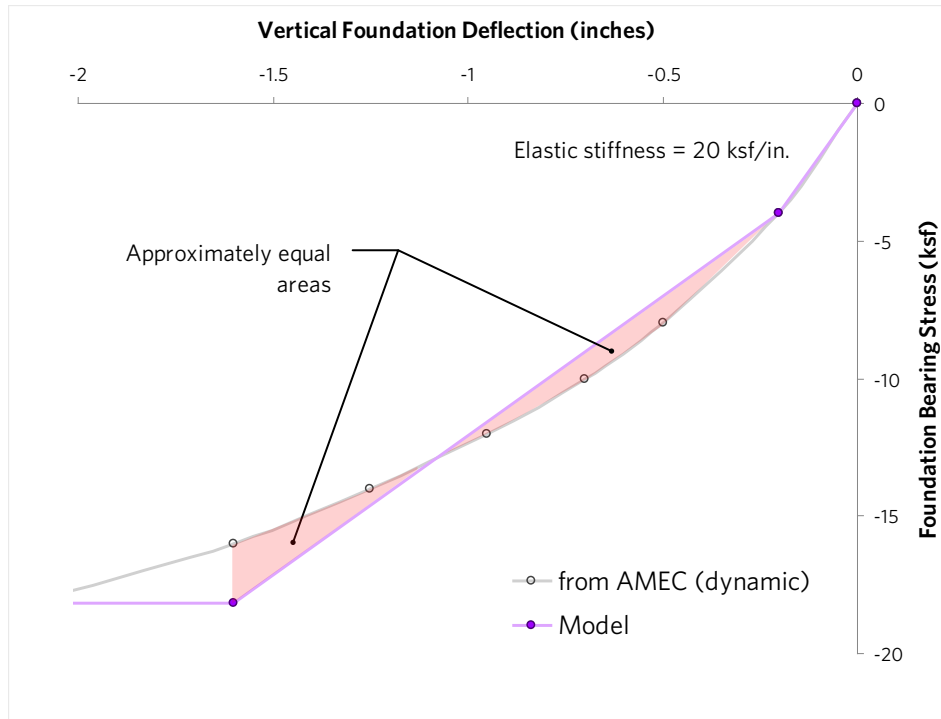


Figure 4-4 Graph of linearized soil material backbone overlaid on a portion of backbone curve from AMEC. The deflection is based on demands from preliminary analysis results.

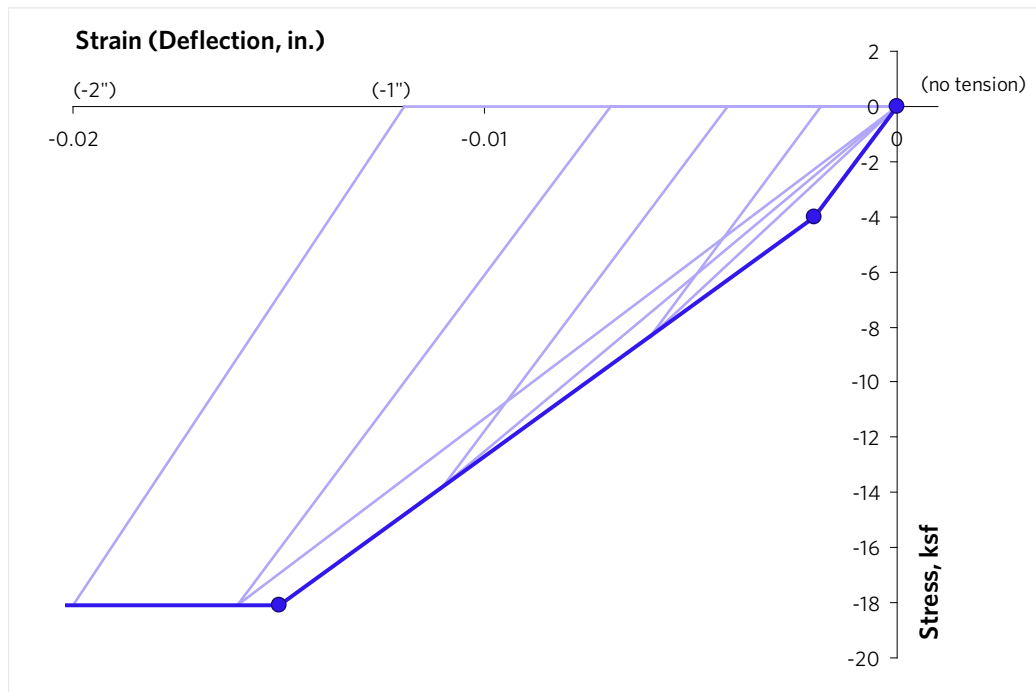


Figure 4-5 Soil material stress-strain curve and hysteresis (calibrated for gage length of 100 inches).

## 5 Components

The components used in the model are described briefly in this section.

### 5.1 Bars

The bar element is a two-node element that tracks only axial forces and deformations; i.e. it cannot resist bending moment nor shear. In model of the monument, two types are employed: elastic bar elements and bar elements assigned a material and area.

#### 5.1.1 Elastic bar elements

Elastic bar components are defined by assigning a modulus of elasticity and area. The component may then be assigned to any number of bar elements. These elements behave elastically so that there is a linear relationship between element force and deformation. Consequently, these elements do not dissipate energy nor do they soften or lose strength, and they can resist tension and compression.

In the model, elastic bar elements are used to transfer forces in places where nonlinear behavior is not expected (and therefore not allowed). These include elements within the foundation and the horizontal restraint elements at the base (see Figure 7-2). These elements are monitored to verify the strength of the component modeled is not exceeded, confirming that the elastic assumption is valid.

#### 5.1.2 Bar elements of specified material

A bar component may be defined by assigning a material and area. The component may then be assigned to any number of bar elements. Given displacements at an element's end-nodes, the compatible axial strain is computed. The stress is recovered from the material depending on its hysteretic behavior and multiplied by the area of the bar component to compute the force that applies to the end-nodes.

Bar elements of this type are used to model the vertical soil below the foundation (see Figure 7-2) and the clamping elements that supplement bearing force on the friction slider elements.

### 5.2 Frame elements

Frame elements are two-node elements that model axial, bending, and shear actions. They are defined by first defining a *Frame Compound Component*, which is a list of sub-components that might include inelastic shear or moment hinges, fiber cross-sections for bending, elastic releases, in addition to a sequence of elastic cross-sections. The compound component may be assigned to any number of frame elements.

In the model of the monument, frame elements do not play a primary role in behavior. There are many frame elements in the model used in conjunction with the wall elements described in the following section. The wall element does not resist "screwing" moment applied to a single node, as would be imposed by friction slider elements (see Figure 5-1). Thus, frame elements are required to properly transfer moments into the wall elements.

There are also frame elements in the pyramidion where the secondary ribs terminate in stone lintels (see Figure 9-2).

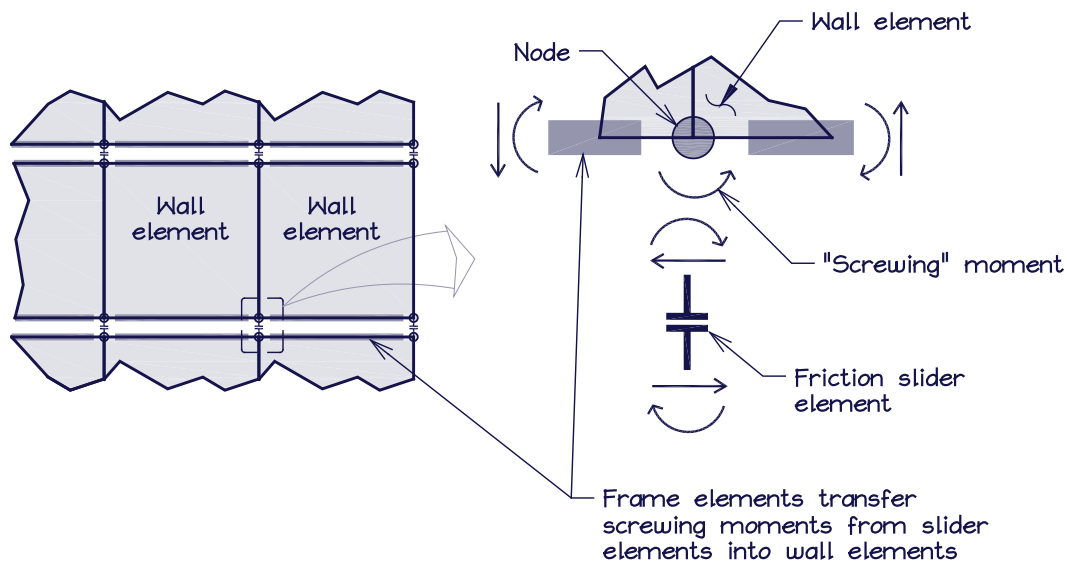


Figure 5-1 Illustration of use of frame elements to transfer "screwing" moments from friction slider elements into wall elements.

### 5.3 Wall elements

Wall elements in the model are four-node elements assigned a *Wall Compound Component*. It comprises four layers of sub-components acting in parallel: two cross-sections to model in-plane bending and axial actions on opposing faces of the element, and two types of shear materials with corresponding thicknesses to model in-plane shear actions. Out-of-plane actions are elastically similar to shells.

#### In-plane bending and axial actions

Each wall element has two sets of opposing edges on which bending moments and axial actions can be applied (Figure 5-2). These moments and axial forces are resolved into equilibrating forces at the nodes of the element. The cross-sections may be modeled elastically or with inelastic potential using fiber cross-sections. In most cases in the monument model, fiber cross-sections are defined by a material assignment, cross-section thickness, and fiber mesh size. The masonry fiber material (described in section 4.1) and thickness depend on the location of the wall element in the model. Each cross-section comprises three (3) fibers. Thus, each side of the tower comprises a row of four (4) elements that model twelve (12) vertical fibers total (see section 8).

The cross-sections are assigned to the two orthogonal directions (i.e. opposing faces of the four-sided element) of the *General Wall Compound Component*, and the compound component is assigned to the wall elements. The definition of the masonry material has the effect of modeling potential cracking in tension that may result from applied bending moment and axial force.

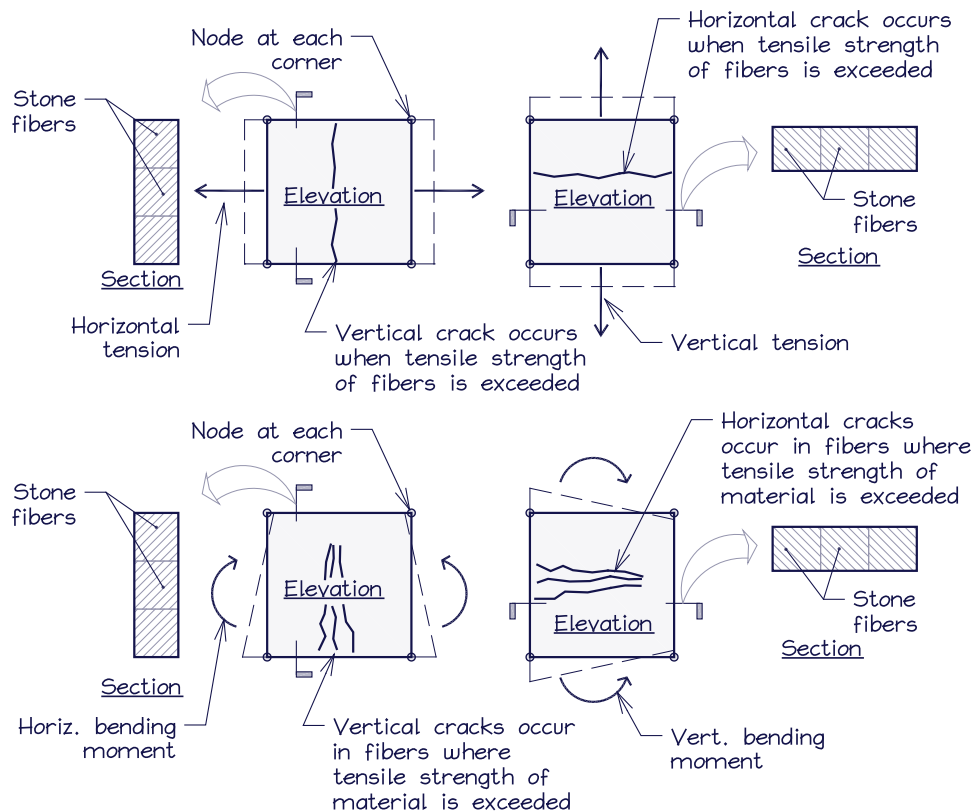


Figure 5-2 Illustration of in-plane bending and axial behavior of the *General Wall Compound Component*.

### In-plane shear

In-plane shear actions are modeled using two types of materials acting in parallel inside the wall element: *Conventional Shear* and *Diagonal Strut* materials (Figure 5-3). The conventional shear material implies a certain tensile strength along the diagonal. Thus, this material is calibrated to lose strength if the corresponding diagonal tensile stress exceeds 100 psi. This emulates a brittle material solid that cracks when the stress limit is reached. Once the shear material in the wall element loses strength, it continues to resist shear through cross-struts acting in compression. Bounding analyses were also run with tensile strength reduced to 20 psi.

The strut material models a pair of cross-struts with compression-only behavior conforming to the assigned material and specified thickness. At the wall nodes, the strut force must equilibrate vertical and horizontal confining forces. Typically the vertical confining force comes from the self-weight of the structure. The horizontal force comes from the nominal tension capacity of the stone material noted in section 4.1.

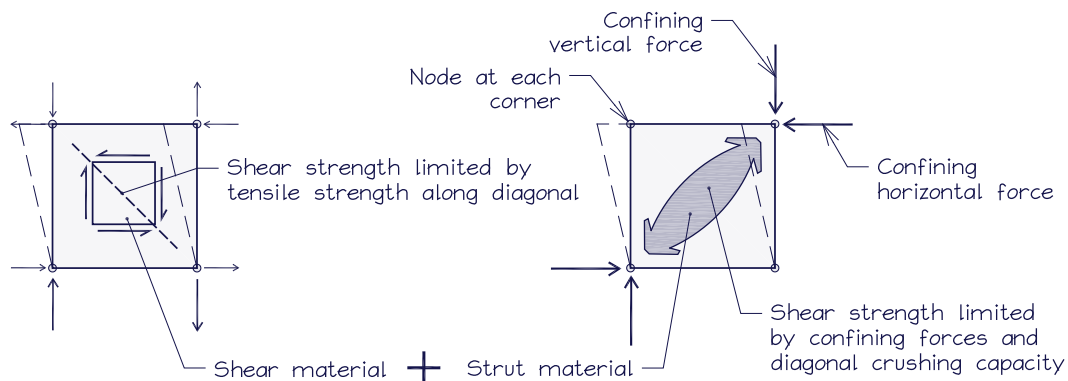


Figure 5-3 Illustration of in-plane shear in the *General Wall Compound Component*.

## 5.4 Frictional sliders

Frictional slider elements are used throughout the model to represent potential sliding surfaces between courses of stone. The principal feature of this element type is that the shear force that causes the element to slip is directly proportional to the bearing force through the friction coefficient. Thus, the propensity to slip will be evaluated and the capacity adjusted dynamically during the analysis. Thus, if a slider element should have its bearing force reduced by the action of overturning moment, its shear capacity is reduced proportionally; conversely, an increase in bearing force due to bending moment leads to a proportional increase in shear capacity.

The slider elements are two-node elements that are assigned a *Friction Pendulum Component* (Figure 5-4). The slider element has a specified friction coefficient and is modeled with a flat (non-pendulum) surface. The lateral stiffness before slipping and axial stiffness in compression are elastic and are calibrated to the area of material represented by the slider element. Tension actions are also elastic, but the stiffness is set to be nominally zero. This allows uplift with little tensile force (note that this type of uplift is akin to the cracking that is also modeled in the wall elements). The orientation of the sliding surface must also be specified, which is used for the sloping interfaces of the stones in the pyramidion (see section 9).

The default behavior of the slider element would lead to zero lateral stiffness and strength if the element were to undergo axial tension. The masonry in the monument is unlikely to behave this way in reality. Rather, two courses of stone would not slide over one another unless the tensile stress exceeds the nominal tensile capacity of the materials (defined in section 4.1). To emulate this behavior, clamping bar elements are modeled in parallel with each slider element. These elements are assigned a tension-only material that loses strength at a stress of 50 psi. The area of each clamping element is set to match the area of stone represented by the slider element. The clamping elements are then pre-tensioned to near 50 psi, thereby applying compressive stress to each slider element in addition to that provided by self-weight. During the analysis, the clamping bar (which was pre-tensioned to near its capacity) would lose strength if the slider element undergoes excess tensile strain, allowing the slider element to slide freely.

The effect of the clamping elements on the slider elements is illustrated in Figure 5-5. In the left graph, the axial compression force of each slider element is plotted with and without the added clamping force. Potential sliding planes are modeled using these elements at a spacing of roughly eight feet

vertically, and there are sixteen (16) slider elements at each plane of potential sliding (except above the 470-foot level). Each element is represented in the graph, so that the sum of the axial forces of the sixteen slider elements equals the total axial force in the monument at a given sliding plane. In the graph on the right, the bearing stress for each element is plotted. Typical bearing stress under gravity loading 200 to 300 psi, and the clamping elements add roughly 50 psi.

The model was also run without the tension effect. A comparison indicates that the elements have little effect on the results and subsequent recommendations. The results with the tension effect are reported in section 13.

Additional analyses were run assuming reduced masonry tensile capacity. In these analyses, the clamping stress was not modeled so that the slider elements were allowed to slide under any amount of tension stress. Selected results from these analyses are reported in section 14.

It is recognized that the friction coefficient is potentially the most critical parameter in the model, yet like the other material properties, it cannot be known precisely. Because stone is a heterogeneous material, two stones of the same material may have different static friction coefficients depending on the roughness of the interfacing surfaces. Friction coefficients for stone are presumed to vary between 0.5 and 0.7. Because of the variability of this parameter and its presumed importance on the behavior and subsequent evaluation, parallel models are analyzed with upper and lower bound assumptions for friction coefficient, similarly to the strength and stiffness properties of the stone (see Section 4.1).

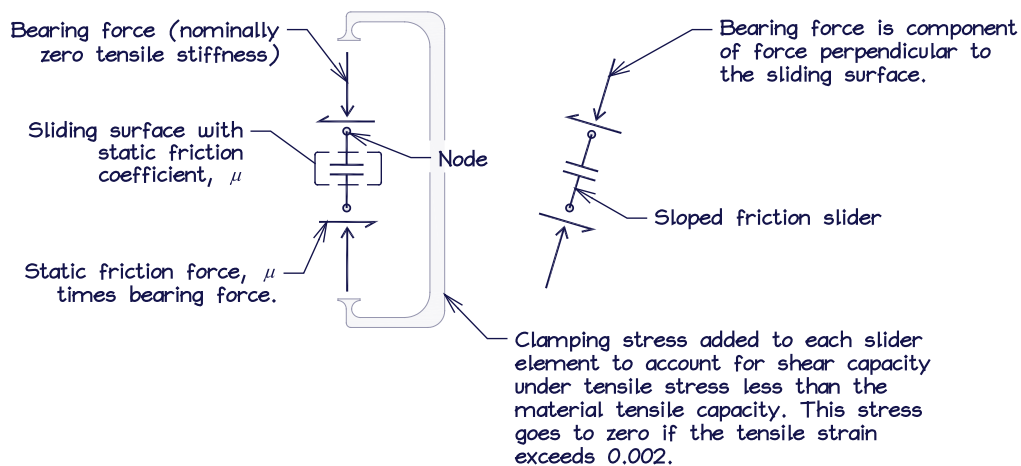


Figure 5-4 Diagram of friction slider element.

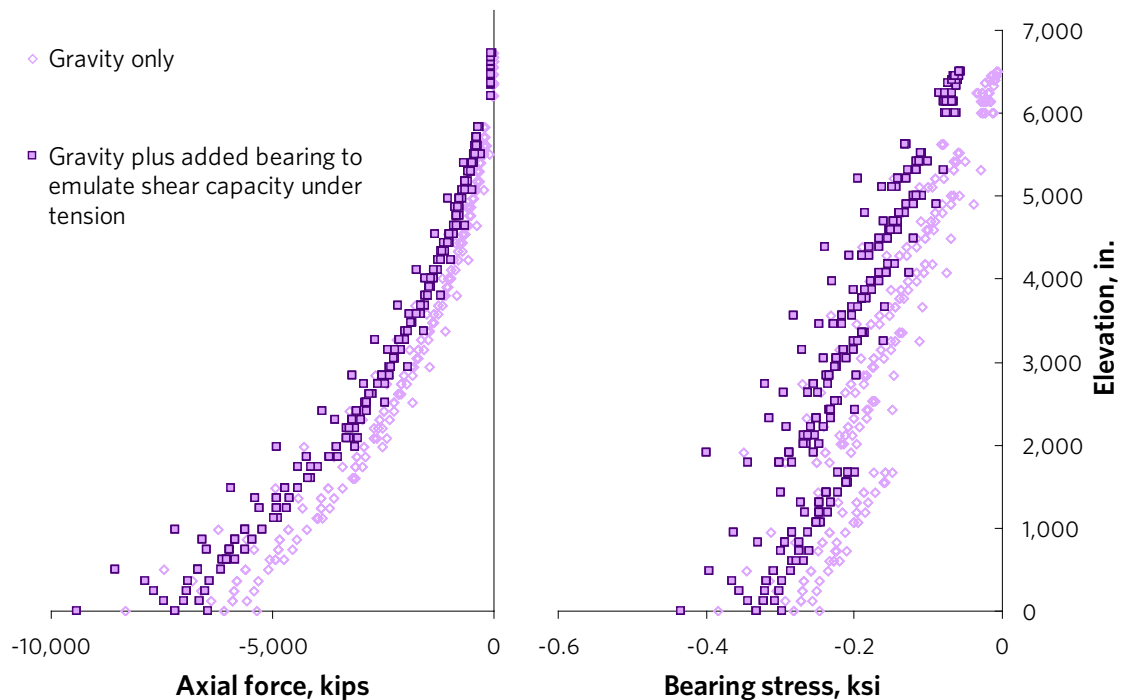


Figure 5-5 Plots of individual slider element bearing force (right) and stress (left) illustrating the effect of the added bearing stress. There are typically sixteen (16) slider elements at each elevation.

## 6 Mass and gravity loading

Mass and gravity loading are defined at elevation increments of 40'-0" below the pyramidion and at four elevations within the pyramidion. The total seismic mass above grade is estimated to be 104,000 kips. Gravity loads of the same values are input above grade, and additional loads are applied to the foundation to properly model soil bearing pressure and to account for resistance against overturning. The total weight of the structure, including the foundation is estimated to be about 177,000 kips. Figure 6-1 shows graphs of the weight distribution and cumulative weight in the model.

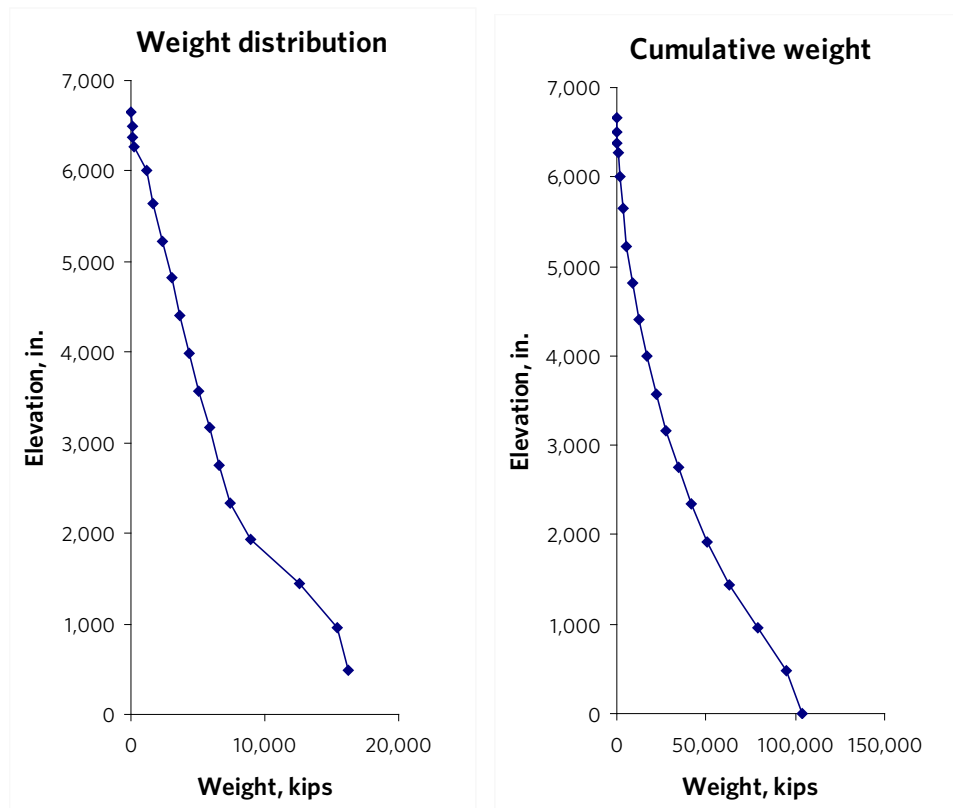


Figure 6-1 Estimate of weight distribution (left) and resulting cumulative weight profile (right).

## 7 Foundation and soil modeling

The monument sits upon a foundation composite of concrete and stone (Figure 7-1). The base of the footing is about 36'-10" below grade and the new underpinning concrete is about 13'-6" thick. The foundation can transfer compression to the soil below and resist overturning moment by tipping on its edge and offsetting the compression resultant.

The foundation has a significantly larger footprint than the base of the tower. It is assumed that any inelastic action occurring near the foundation would be in the soil or in the tower, but not in the foundation itself, given the size of the foundation relative to the tower at the base and given the strength of the foundation relative to the soil below. Therefore, the foundation is modeled elastically and supported by vertical bar elements assigned compression-only soil material with nonlinear potential as shown in Figure 7-2. This configuration allows the footing to rock on its edges without transferring fictitious tensile forces into the soil. Each of the soil elements is assigned a tributary area of soil as illustrated in Figure 7-3 and the material described in section 4.2. Horizontal restraint is provided at grade and at the base of the footing by stiff elastic bar elements.

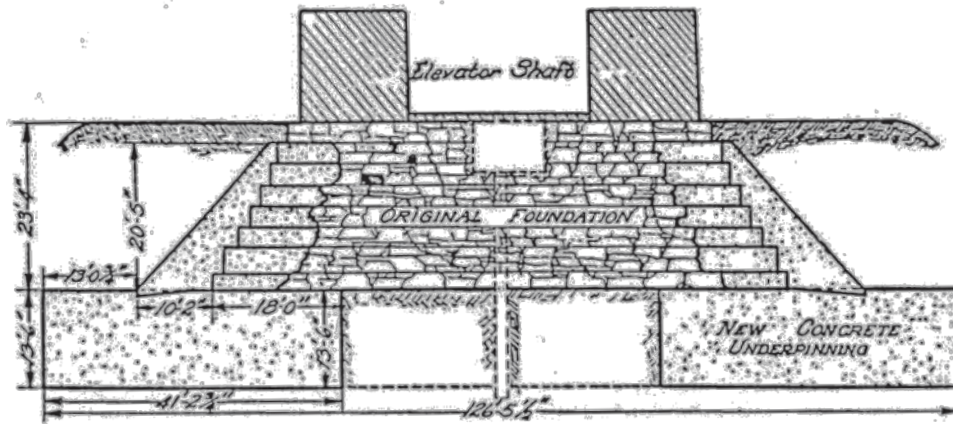


Figure 7-1 Section of foundation (Society of American Military Engineers, The Washington Monument, 1929). Excerpted from Figure 1 of the evaluation report by Oehrlein and Associates Architects, 1993.

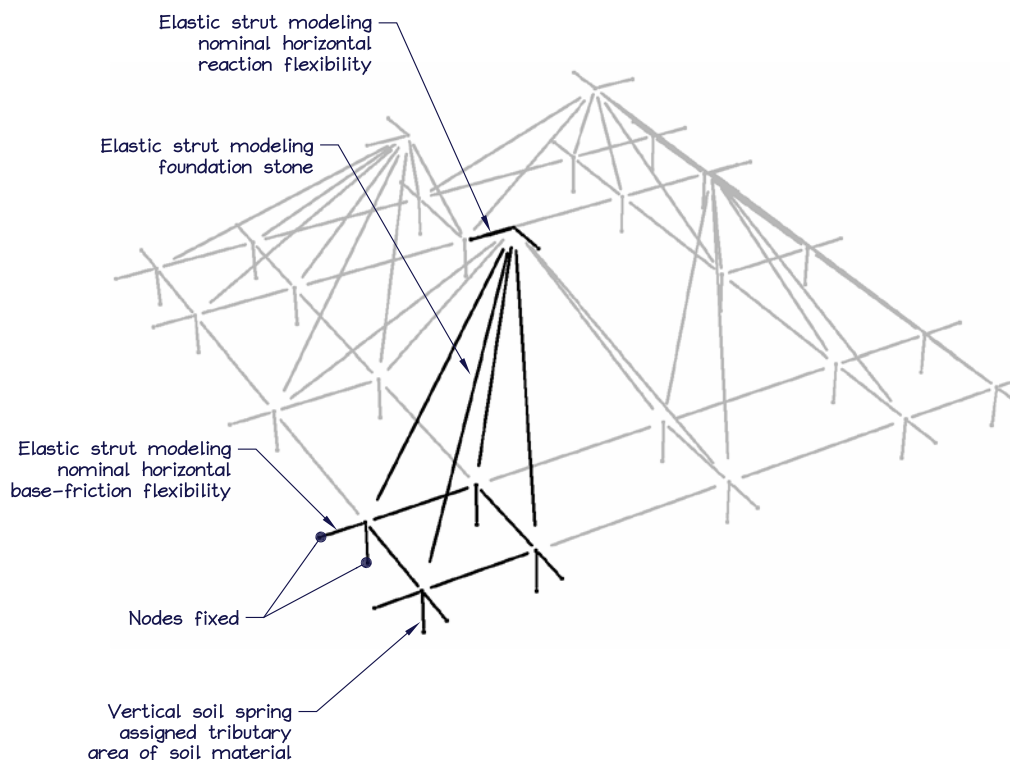


Figure 7-2 Illustration of soil and foundation elements in model.

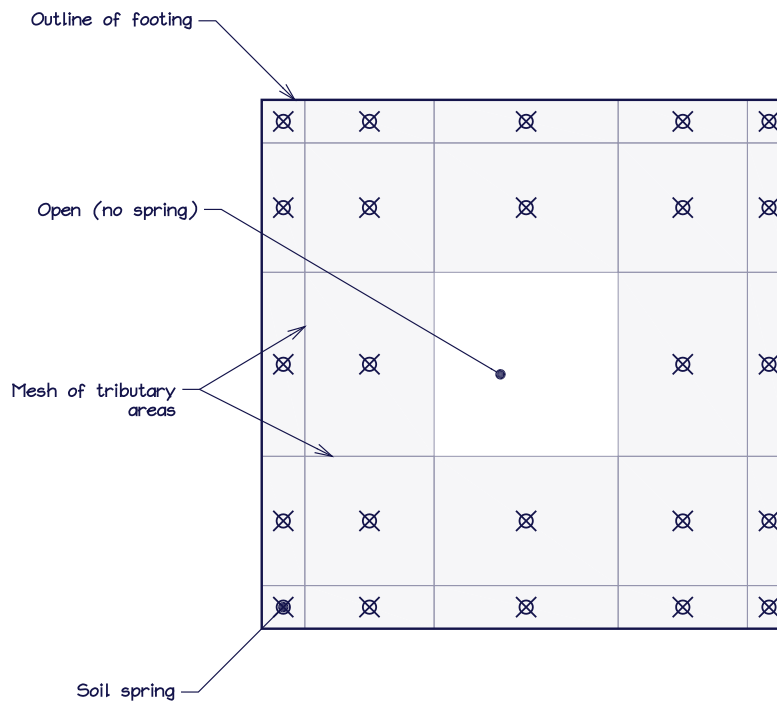


Figure 7-3 Plan view of soil springs illustrating tributary areas of soil.

## 8 Modeling of the tower below 470 feet

The tower below the 470-foot level is fairly regular; it is modeled in a repeating pattern of wall elements separated by slider elements (see Figure 8-1). There is a significant transition in wall thickness occurring at an elevation of about 160 feet, and this is accounted for in the sizes assigned to the various elements. This modeling approach allows for potential slipping to occur at many elevations. Figure 8-1 illustrates the equilibrium forces at the nodes above and below a slider element. It shows that the force  $P\mu$  relies upon tensile capacity of the stone to activate sliding. If the available tensile force is less than  $P\mu$ , the model would indicate a vertical crack in the wall element. Both potential sliding and vertical cracking actions are modeled explicitly. The stair construction in the tower was not modeled because its stiffness is insignificant in comparison to the masonry.

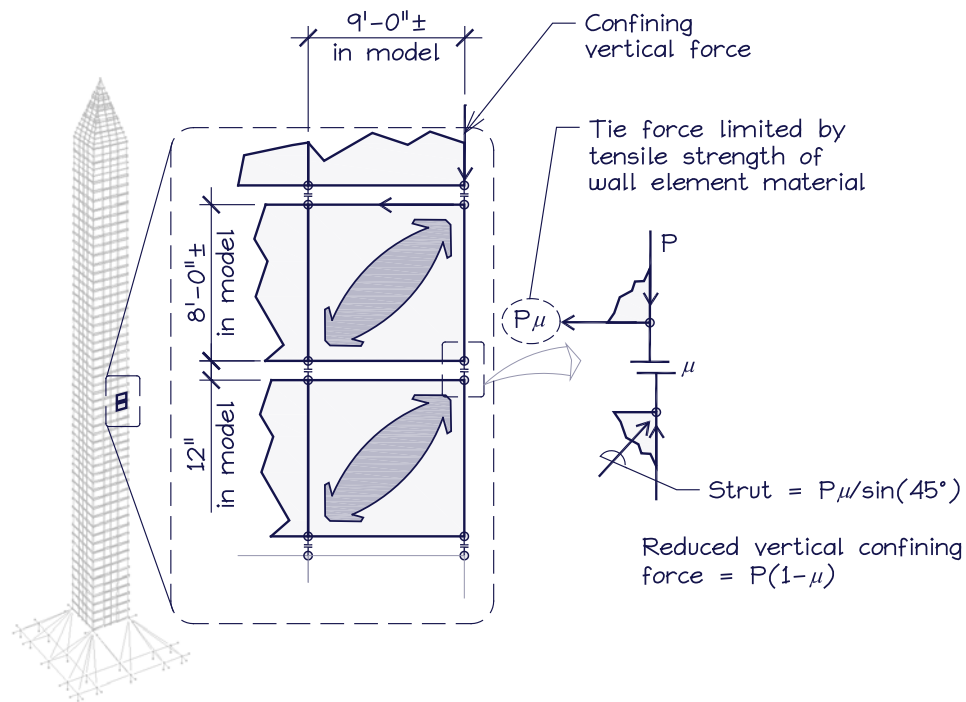


Figure 8-1 Illustration of tower modeling below the 470-foot level and the forces at a typical node under a potential sliding condition.

## 9 Modeling of the pyramidion

The ribs are built integrally with the wall and spring from about the 470-foot elevation (Figure 9-1 and Figure 9-2). In the model, the mesh of elements transitions so that nearly each stone (as illustrated in the Oehrlein report) has assigned its own wall element. These wall elements are assigned stone material without tensile strength. Between each three levels of wall elements is a set of friction slider elements to model potential sliding at the interfaces between stones. Both the center and side sets of ribs are modeled in each direction, including the requisite intersections.

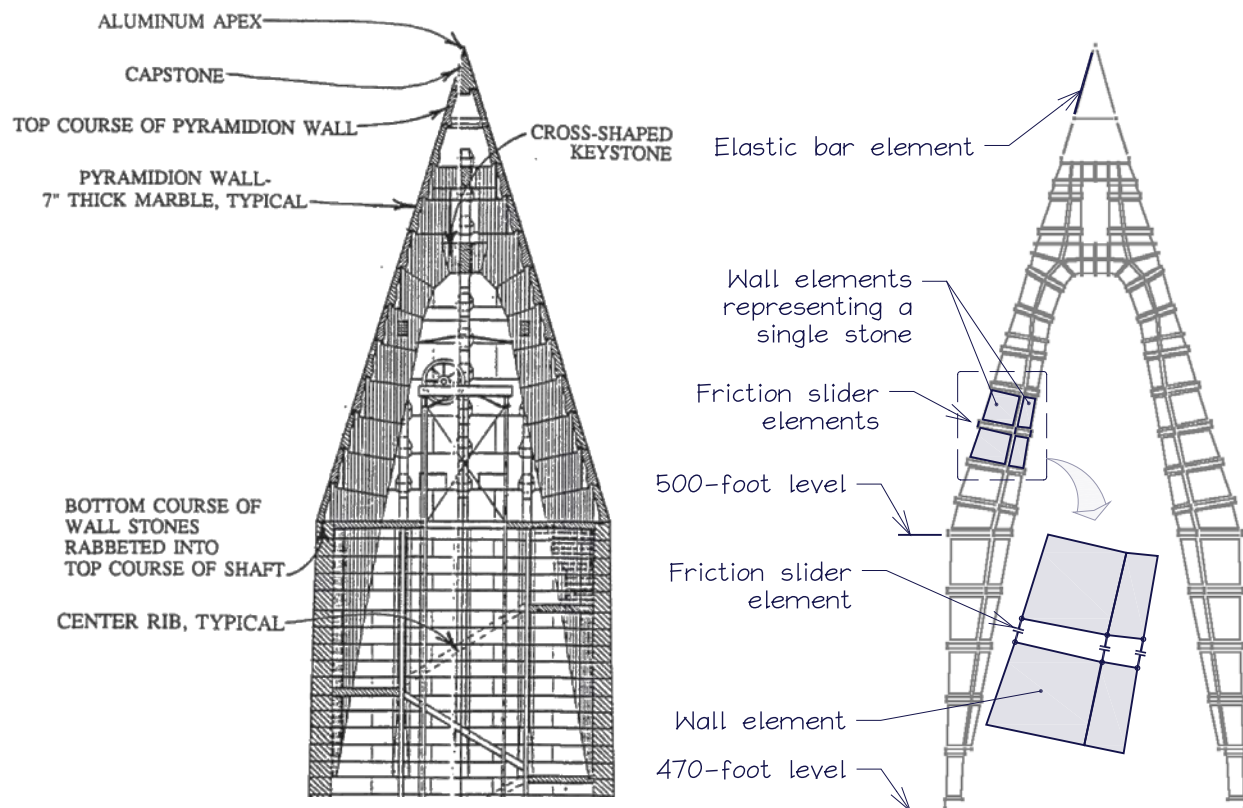


Figure 9-1 Left, section of pyramidion at center (primary) rib (drawing by Engineering Office of the Washington Monument, Thomas Lincoln Casey Engineer in Charge, 1884. National Archives, Record Group 79. Excerpted from Figure 11 of the evaluation report by Oehrlein and Associates Architects, 1993). Right, screen-shot showing elements from the model.

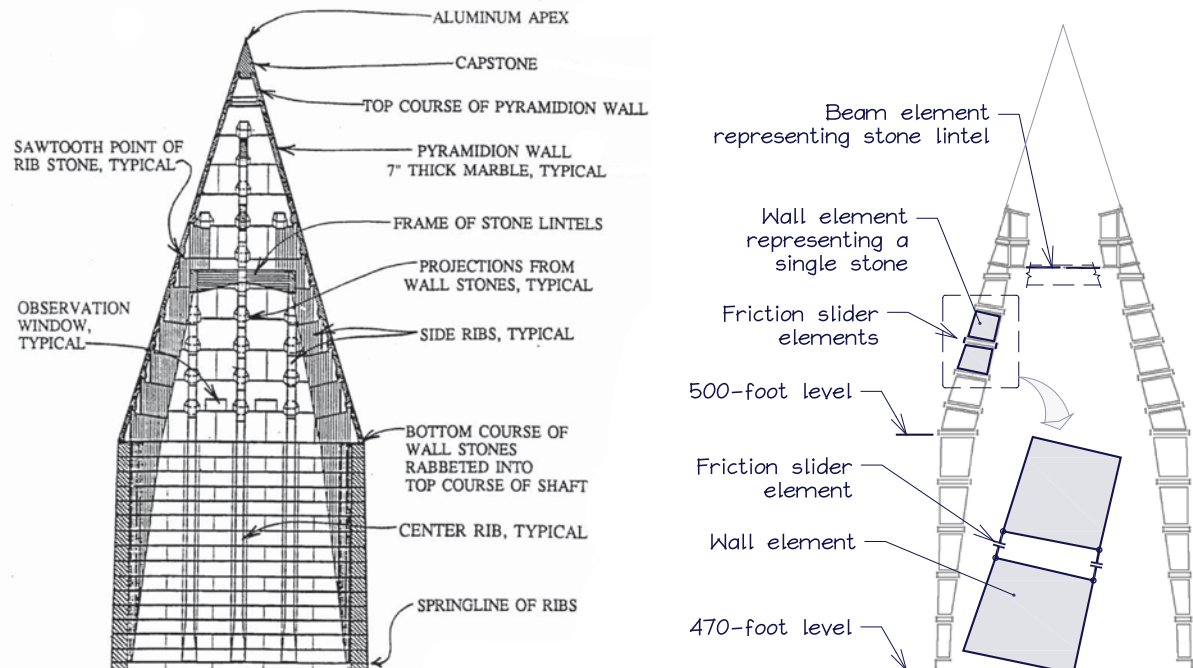


Figure 9-2 Left, section of pyramidion at side (secondary) rib (drawing by Engineering Office of the Washington Monument, Thomas Lincoln Casey Engineer in Charge, 1884. National Archives, Record Group 79. Excerpted from Figure 11 of the evaluation report by Oehrlein and Associates Architects, 1993). Right, screen-shot showing elements from the model.

The outer surface of the pyramidion is modeled to integrate with the modeling of the ribs (Figure 9-3). The wall elements are assigned 7" thickness of stone material. As with the ribs, there is a set of slider elements between each third row of wall elements. At the 470-foot elevation a fictitious beam is modeled to transfer the forces from interior wall elements above to the corner elements below.

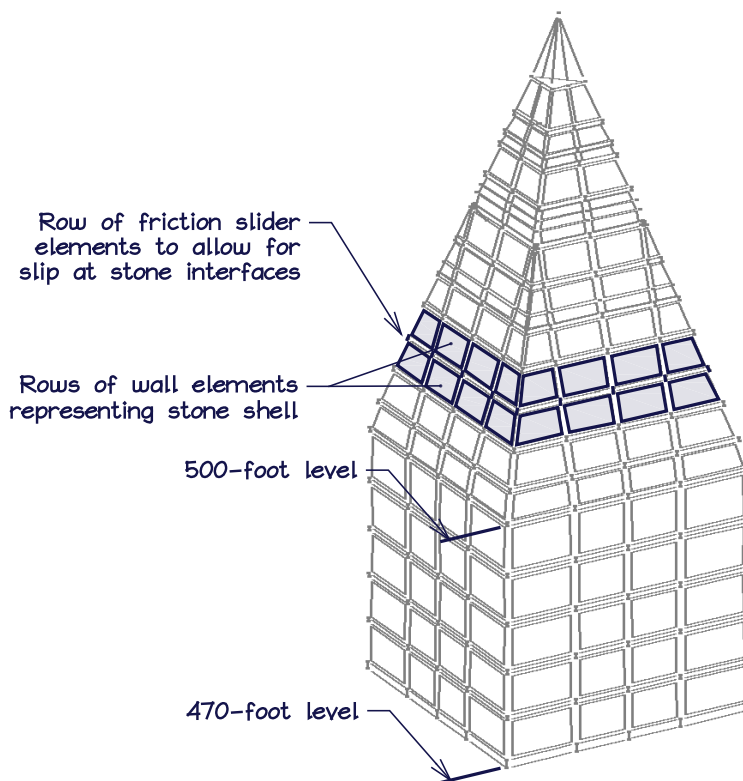


Figure 9-3 Screen-shot showing elements from the model in the shell of the pyramidion.

## 10 Viscous damping

Viscous damping is modeled using the Rayleigh damping model (a.k.a.  $\alpha$ - $M$ ,  $\beta$ - $K$ ) in which a suitable damping matrix is constructed through a linear combination of the mass and stiffness matrices. This implies a constraint on the damping in which damping depends on the period of the vibration mode under consideration. Rayleigh damping may be determined by specifying the damping ratio as a percentage of critical damping at two periods. The model has 3% and 1% of critical damping at periods of  $0.2 T$  and  $1.0 T$ , respectively, where  $T$  is the period of the vibration mode under consideration. The resulting damping curve is illustrated in Figure 10-1.

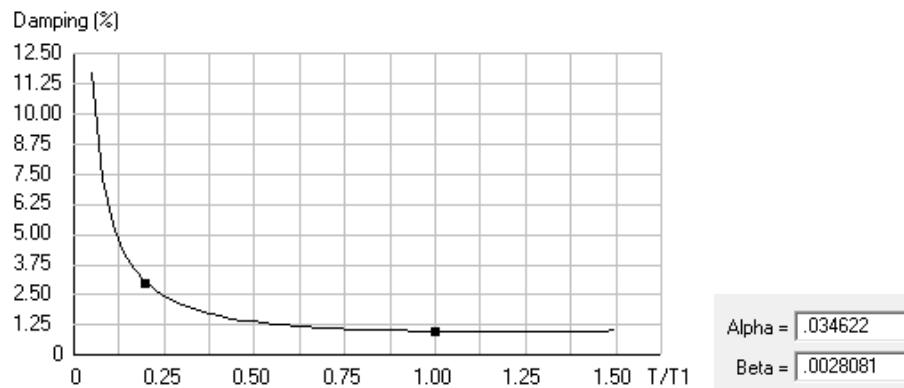
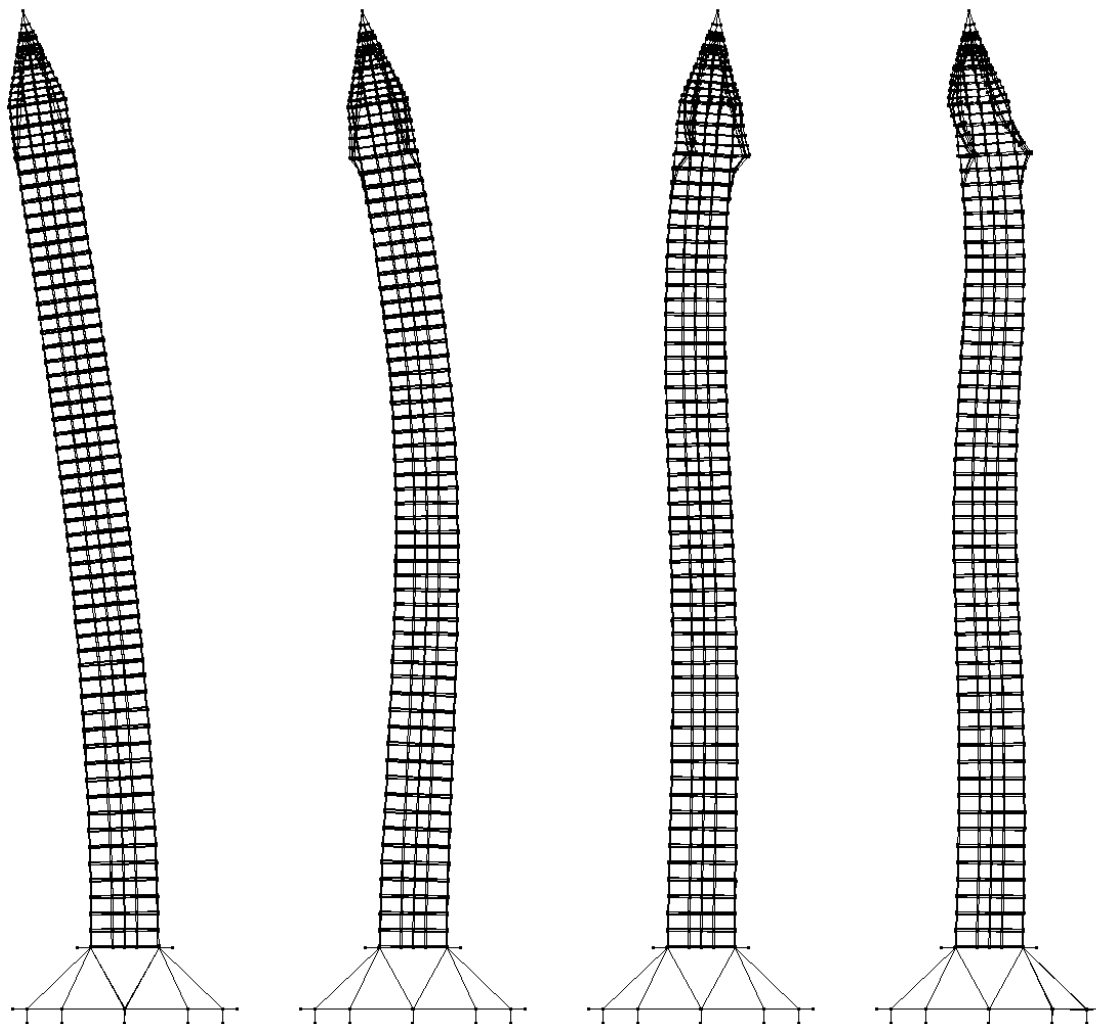


Figure 10-1 Screen-shot from Perform of graph illustrating Rayleigh damping parameters.

## 11 Elastic modes of vibration

The model is analyzed to find the elastic modes of vibration and corresponding periods. The first four translational modes are illustrated and the periods listed for the lower and upper bound assumptions for stone stiffness in Figure 11-1. Varying the friction coefficient of the slider elements has little effect on the modes. Identical modes occur in the perpendicular direction. Around 90% of the effective mass is included in the first four modes. The periods range between 2.55 seconds and 0.21 seconds for the softer version of the model and 2.01 seconds and 0.18 seconds for the stiffer version.

The predicted periods of vibration are somewhat different than those predicted by *WJE*. However, these differences are within normal tolerances considering the different software and different modeling approaches employed. Also, the differences in periods imply that a greater range of potential behavior is considered. Thus, the two approaches compliment each other and together bound a larger spectrum of possible behavior than either approach would do alone.



Mode	Lower bound material stiffness		Upper bound material stiffness	
	Period, sec.	Mass participation	Period, sec.	Mass participation
1	2.55	46%	2.01	47%
2	0.68	25%	0.57	25%
3	0.34	12%	0.30	12%
4	0.21	6%	0.18	4%

Figure 11-1 First four elastic modes of vibration and corresponding periods for the lower and upper bound assumptions for stone stiffness.

## 12 Ground motions and seismic hazard

The nonlinear response history analysis relies on ground acceleration input that corresponds to the seismic hazards of interest. For this purpose, ground accelerations were selected by geotechnical

engineers, AMEC Environment & Infrastructure to represent two hazards, the Mineral, Virginia earthquake and the Maximum Considered Earthquake (MCE). These hazards are the subject of the following two sections.

## 12.1 Mineral, Virginia

One set of ground accelerations represents the shaking that occurred during the earthquake that originated near Mineral, Virginia in August, 2011. There are no ground accelerometers at the monument itself, but there are several in the near vicinity. The development of the acceleration records by AMEC is based on both probabilistic and deterministic representations of seismic hazard. The computed target acceleration response spectrum was compared with those calculated from the records at nearby sites. This comparison showed similarities in spectral shape, but the records indicate that larger accelerations may have occurred at the monument in certain period ranges. Figure 12-1 is a map showing the epicenter (lime green) and the monument (red) about 131 kilometers away. There are three other pins on the map showing sites where ground motions were recorded by the USGS.

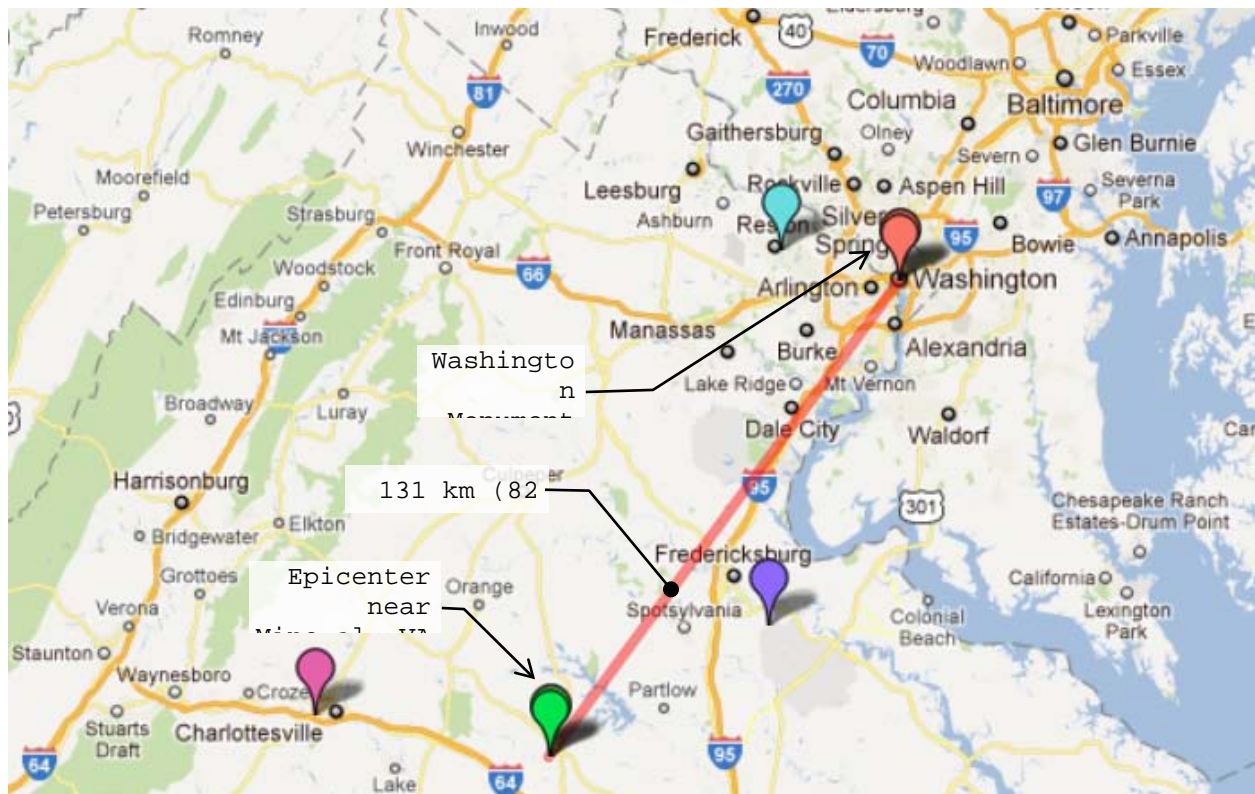


Figure 12-1 Map showing Mineral, Virginia earthquake relative to the Washington Monument.

The acceleration response spectra for the seven selected ground motions are plotted in Figure 12-2. There is one graph for each record, taking the SRSS (square-root of the sum of the squares) of the motions in the two orthogonal directions. The average of the peak ground accelerations (on the plot at period of zero seconds) is about 0.12g seconds. The largest mean spectral acceleration occurs at a period of 0.26 seconds is 0.34g, and it drops off sharply for longer periods. In the model, the acceleration components of the two orthogonal directions are analyzed simultaneously.

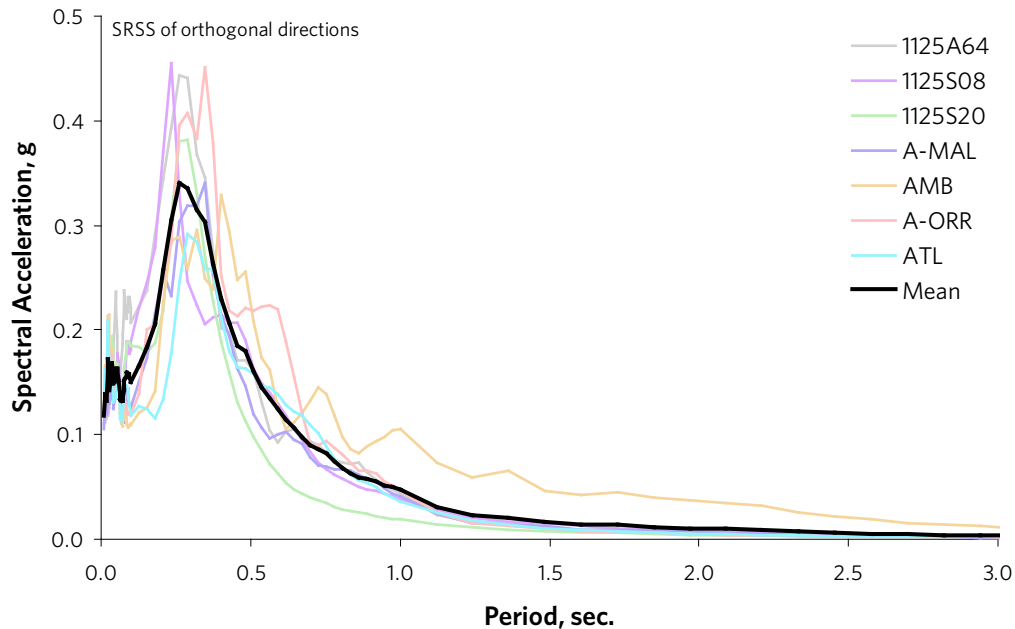


Figure 12-2 Acceleration response spectra for the seven selected ground motions representing the Mineral, Virginia hazard. There is one graph for each record, taking the SRSS of the motions in the two orthogonal directions.

## 12.2 MCE

The geotechnical engineer also selected ground motions to represent the Maximum Considered Earthquake (MCE). As the name suggests, this hazard represents the largest intensity of shaking that is to be considered at the site. It is supposed to take into account regional seismicity and site-specific geotechnical conditions that may affect the shaking at the ground surface. The acceleration response spectra for the seven selected ground motions are plotted in Figure 12-3. There is one graph for each record, taking the SRSS of the motions in the two orthogonal directions. The average of the peak ground accelerations (on the plot at period of zero seconds) is about 0.12g seconds, which is the same as the Mineral hazard. The largest mean spectral acceleration occurs at a period of 0.29 seconds is 0.31g, and it plateaus for longer periods at a value of around 0.062g, which is much larger than the Mineral hazard for larger periods. In the model, the acceleration components of the two orthogonal directions are analyzed simultaneously.

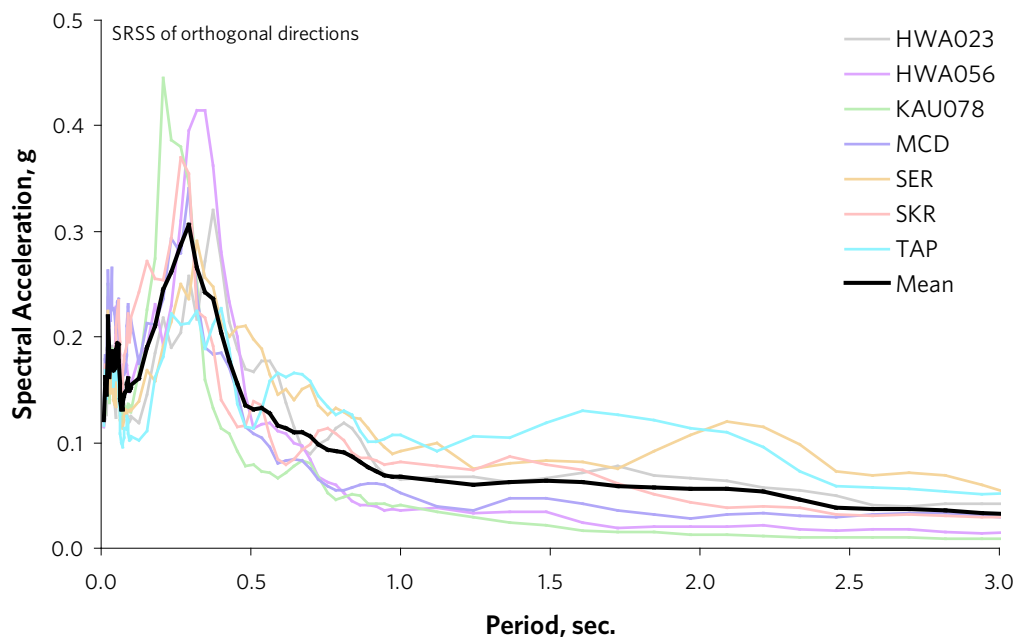


Figure 12-3 Acceleration response spectra for the seven selected ground motions representing the MCE hazard. There is one graph for each record, taking the SRSS of the motions in the two orthogonal directions.

### 12.3 Record names

The selected records come from various earthquakes and recording sites. This information is summarized in Table 12-1. Because distinguishing among the records can be difficult, short-hand names are assigned to each record as indicated in the right-most column. The short-hand names are used throughout this report.

Table 12-1 Table of earthquake records. The right-most column indicates the short-hand names used throughout this report.

Earthquake	Year	Recording station	Short name
<b>Mineral</b>			
Saguenay	1988	ECTN:A64	1125A64
Saguenay	1988	GSC Site 8 - La Malbaie, Que	1125S08
Saguenay	1988	GSC Site 20 - Les Eboulements	1125S20
Whittier Narrows	1987	Malibu - Point Dume Sch	A-MAL
Georgia, USSR	1991	Ambralauri	AMB
Whittier Narrows	1987	Castaic - Old Ridge Route	A-ORR
N. Palm Springs	1986	Anza - Tule Canyon	ATL
<b>MCE</b>			
Chi-Chi, Taiwan	1999	HWA023	HWA023
Chi-Chi, Taiwan	1999	HWA056	HWA056
Chi-Chi, Taiwan	1999	KAU078	KAU078
Kocaeli, Turkey	1999	Mecidiyekoy	MCD
Landers	1992	Villa Park - Serrano Ave #	SER
Duzce, Turkey	1999	Sakarya	SKR
Chi-Chi, Taiwan	1999	TAP060	TAP060

## 12.4 Comparison

The mean spectra for the Mineral and MCE hazards are plotted in Figure 12-4 for comparison. The graph shows that the Mineral hazard has, on average, larger spectral accelerations up to a period of about 0.6 seconds. At larger periods, the MCE hazard shows larger accelerations including a broad plateau between periods of about 1.0 seconds to 2.2 seconds at which the spectral acceleration is about 0.062g. The spectral acceleration for the Mineral hazard over this period range is roughly about 25% of this, or 0.014g. This implies that modes of deformation associated with shorter periods (higher frequency) would generally be excited more by the Mineral records while those associated with longer periods (smaller frequency) would be excited more by the MCE records. Considering elastic modes discussed in section 10, excitation of the pyramidion is likely to be larger under the Mineral hazard than the MCE, while global movement would be expected to be larger under the MCE.

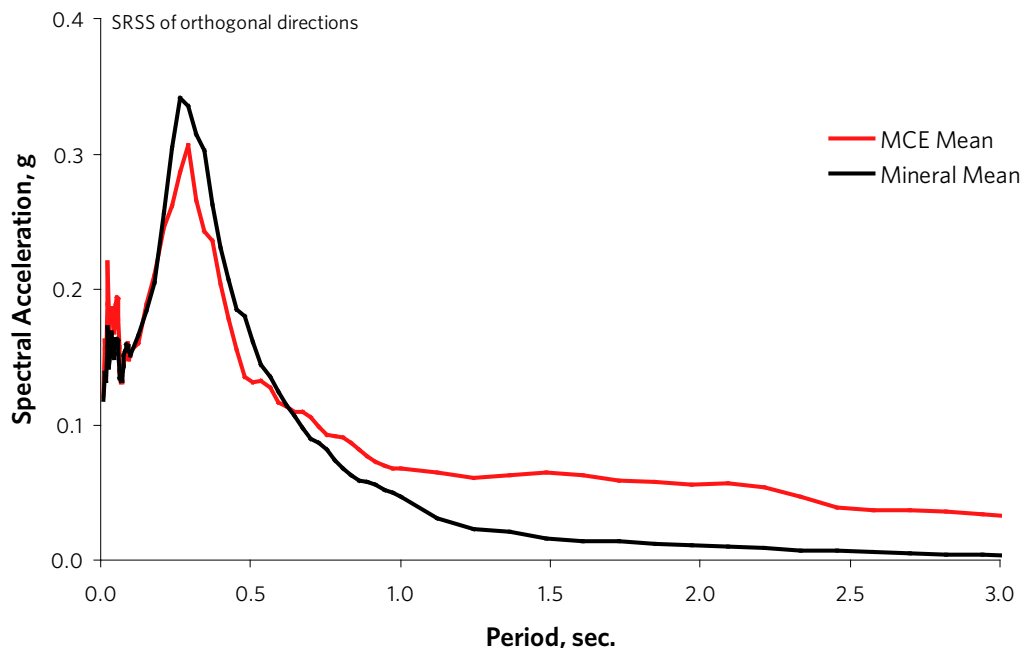


Figure 12-4 Comparison of the mean acceleration response spectra for the MCE and Mineral, Virginia hazards.

## 13 Analysis results

Nonlinear response history analyses were run for two sets of seven earthquakes representing the hazards discussed in section 12. This section provides details of the structural response, quantified in terms of global movement, frictional sliding, soil deformation, and other aspects of elemental damage.

To account for uncertainty in the seismic demand, a set of seven ground acceleration records are analyzed at each hazard level. The structural response will vary depending on the record, leading to a dispersion in response quantities. The mean response of the seven records best-characterizes the seismic performance. Results from all seven records are included to convey the spread of the results. Conclusions and recommendations are drawn from the mean results. The model exhibited stable

behavior under all analyses, including those with maximum response. This a necessary condition validating the use of the mean.

As discussed in the previous sections, uncertainties in the stiffness and strength of the stone and the coefficient of friction are handled by creating four versions of the model. This way, the real properties of the monument are expected to reside somewhere among the permutations analyzed. For each response parameter, results of all four models are reported. The abbreviations "LB" and "UB" refer to lower and upper bound assumptions for the stone stiffness and strength, respectively. The abbreviation "mu" refers to the friction coefficient (commonly represented by the Greek letter  $\mu$ ).

### **13.1 Displacement response**

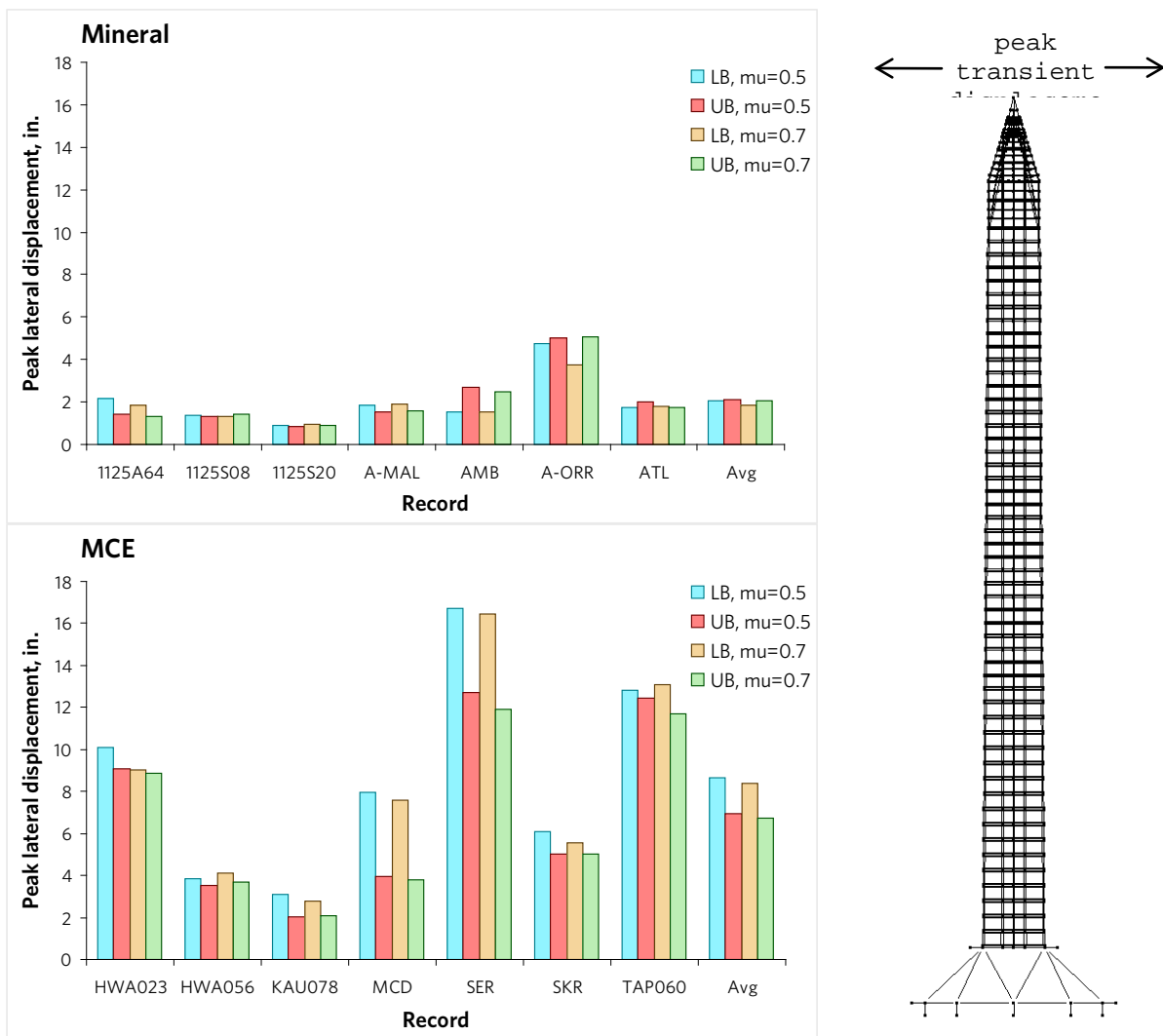
Peak transient displacements at the top of the monument are recovered from the analysis results for each of the four permutations of the model. The results are summarized in Figure 13-1, which shows the peak transient displacement response for each record and model and the average of the records on the far right. In general, the displacements are very small relative to the height of the monument. The largest transient displacement for any MCE record is 16.7 inches, or 0.3% of its height. Allowable limits on this quantity for a typical new building would be about five times larger: on the order of 1% or 2%. The displacement response under the MCE hazard is significantly larger than response under the Mineral hazard. The average response for the MCE (7.7 inches) is nearly four times that of the Mineral hazard (2.0 inches). These displacements are accommodated by the monument elastically for the most part. Some elements in the model undergo inelastic lateral deformations as discussed in the following sections.

At the MCE level, there appears to be some correlation in which the models with the lower bound assumptions for stone stiffness and strength (LB) tend to show larger displacements than those with the upper bound assumption.

Variation in the friction coefficient appears to have little effect on the displacement response. Models with the different friction coefficients show average displacement results within 10% of one another.

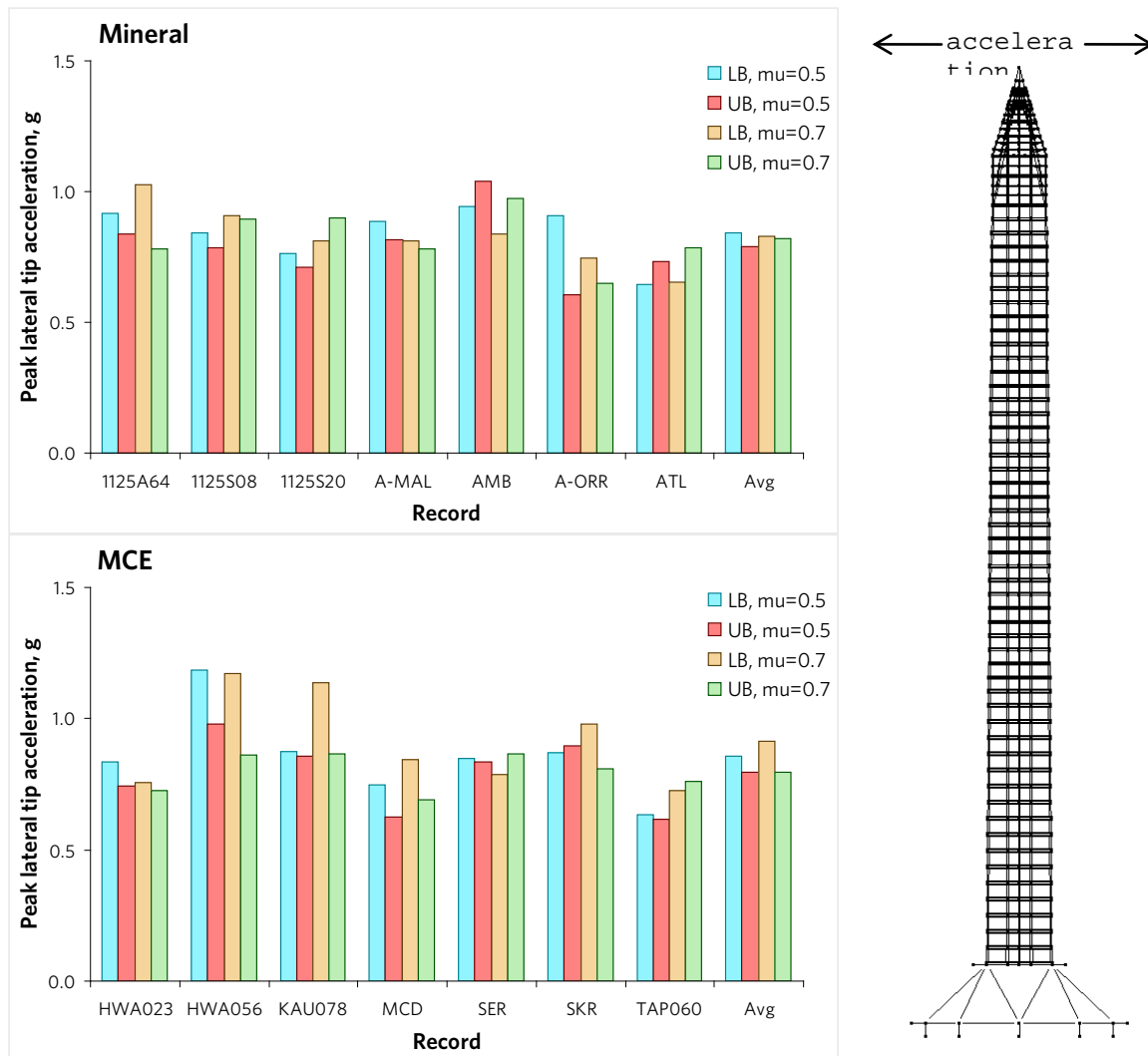
### **13.2 Acceleration response**

Peak acceleration results at the top of the pyramidion are summarized in Figure 13-2, which shows the response in units of  $g$  for each record and model and the average of the records on the far right. The peak acceleration values range between about 0.6 $g$  to 1.2 $g$ . The responses to the Mineral and MCE hazards are similar with average accelerations over all model permutations around 0.8 $g$ . There is no obvious trend correlating acceleration response with variation in material properties in the bounding analyses.



Hazard	Model	Record 1	Record 2	Record 3	Record 4	Record 5	Record 6	Record 7	Avg	$\sigma$	COV
		1125A64	1125S08	1125S20	A-MAL	AMB	A-ORR	ATL	Avg		
Mineral	LB, $\mu=0.5$	2.17	1.35	0.89	1.87	1.54	4.73	1.72	2.04	1.25	0.61
Mineral	UB, $\mu=0.5$	1.45	1.33	0.87	1.55	2.70	5.03	1.98	2.13	1.40	0.66
Mineral	LB, $\mu=0.7$	1.83	1.31	0.95	1.92	1.52	3.77	1.79	1.87	0.90	0.48
Mineral	UB, $\mu=0.7$	1.34	1.42	0.91	1.59	2.49	5.07	1.76	2.08	1.40	0.67
Mineral	Avg	1.70	1.35	0.91	1.73	2.06	4.65	1.81	2.03	1.24	0.61
		HWA023	HWA056	KAU078	MCD	SER	SKR	TAP060	Avg	$s$	COV
MCE	LB, $\mu=0.5$	10.11	3.86	3.09	7.97	16.73	6.08	12.81	8.66	4.93	0.57
MCE	UB, $\mu=0.5$	9.09	3.55	2.01	3.93	12.72	5.00	12.47	6.97	4.42	0.63
MCE	LB, $\mu=0.7$	9.05	4.11	2.80	7.60	16.45	5.54	13.08	8.38	4.93	0.59
MCE	UB, $\mu=0.7$	8.86	3.70	2.08	3.77	11.93	5.00	11.68	6.72	4.05	0.60
MCE	Avg	9.28	3.81	2.50	5.82	14.46	5.41	12.51	7.68	4.58	0.60

Figure 13-1 Graphs and tabular data of peak transient displacement results at the top of the monument in inches: above, for the Mineral hazard and below, for the MCE hazard. Values are the maximum displacement occurring during each record.



Hazard	Model	Record 1	Record 2	Record 3	Record 4	Record 5	Record 6	Record 7	Avg	$\sigma$	COV
		1125A64	1125S08	1125S20	A-MAL	AMB	A-ORR	ATL	Avg		
Mineral	LB, $\mu=0.5$	0.92	0.84	0.77	0.89	0.94	0.91	0.65	0.84	0.11	0.12
Mineral	UB, $\mu=0.5$	0.84	0.79	0.71	0.82	1.04	0.61	0.73	0.79	0.13	0.17
Mineral	LB, $\mu=0.7$	1.03	0.91	0.81	0.81	0.84	0.74	0.65	0.83	0.12	0.14
Mineral	UB, $\mu=0.7$	0.78	0.90	0.90	0.78	0.98	0.65	0.79	0.82	0.11	0.13
Mineral	Avg	0.89	0.86	0.80	0.82	0.95	0.73	0.70	0.82	0.12	0.14
		HWA023	HWA056	KAU078	MCD	SER	SKR	TAP060	Avg		
MCE	LB, $\mu=0.5$	0.84	1.18	0.88	0.75	0.85	0.87	0.64	0.86	0.17	0.20
MCE	UB, $\mu=0.5$	0.75	0.98	0.86	0.63	0.84	0.90	0.62	0.79	0.14	0.17
MCE	LB, $\mu=0.7$	0.76	1.17	1.14	0.84	0.79	0.98	0.73	0.91	0.18	0.20
MCE	UB, $\mu=0.7$	0.73	0.86	0.86	0.69	0.87	0.81	0.76	0.80	0.07	0.09
MCE	Avg	0.77	1.05	0.93	0.73	0.83	0.89	0.69	0.84	0.14	0.17

Figure 13-2 Graphs of peak acceleration results at the top of the monument, in units of g: above, for the Mineral hazard and below, for the MCE hazard. Values are the maximum acceleration occurring during each record.

### **13.3 Lateral deformations**

Peak transient and residual lateral deformation results were recovered from the slider elements for each record, model, and hazard. Peak values represent transient lateral sliding that may be expected to occur in the monument during an earthquake. Peak transient deformations of the model are important indicators for assessing local and overall stability of the monument. The residual deformation results are more relevant than the transient for purposes of benchmarking the model against the damage observed from the Mineral earthquake and for assessing seismic performance under the MCE. Overall, none of the permutations of the model showed transient deformations that would be problematic for stability. Furthermore, residual deformations under the Mineral hazard are small, within the range of the cracks observed in the monument, some of which existed before the earthquake.

Peak transient and residual results are summarized in Figure 13-3 and Figure 13-4, respectively, which show lateral deformations as they occur along the height of the monument. There are typically sixteen (16) slider elements at each elevation. The largest deformation occurring at each elevation is represented in the plot. In the graphs, larger, darker markers indicate the mean response of the seven records; lighter, smaller markers indicate results from each record.

The peak transient deformations predicted for the Mineral hazard are significant in the pyramidion but typically zero below, except at one location just below the 400-foot elevation for certain permutations of the model. At this elevation, there are mean inelastic deformations ranging between zero and 0.3 inches depending on the permutation of the model under consideration. Models with upper bound stone stiffness tend to show larger deformations than those with lower bound stiffness. The residual deformation shown in Figure 13-4 at this location is somewhat less. Following the Mineral earthquake, it was observed that the joints between stones in the same course widened, but there were no significant offsets observed below the pyramidion. The deformations resulting from the analysis are small for all permutations of the model, especially considering the scale of the structure.

In contrast with the results of the Mineral analyses, the MCE hazard show small deformations spread more widely throughout the height of the monument in addition to the pyramidion. Lateral deformations in the graph do not represent an offset of the entire tower. Rather, the deformations normally connote a twisting pattern of movement. The plots illustrate a dispersion of deformations over a great height, so that the deformation at any one location is limited. Where nonlinear deformations occur below the 400 foot elevation, the mean transient value is between one-half inches and one inch, depending on the permutation of the model. The corresponding residual deformations are less than the transient, with values ranging between zero and 0.5 inches. There is less variation in residual deformation among the permutations of the model. The change in construction at the 160-foot level appears to not be associated with any nonlinear response.

Figure 13-5 and Figure 13-6 show envelopes of the peak transient and residual deformations, respectively, for each record and the average of the seven records. The largest deformation anywhere in the monument is plotted. They compliment Figure 13-3 and Figure 13-4 to indicate which particular record is causing which amount of lateral deformation. The largest of the mean transient nonlinear values are between zero and 0.3 inches for the Mineral hazard and between 0.5 inches and 1.0 inch for the MCE, depending on the permutation of the model. There are some clear outliers; for example, the MCE-SER record shows significantly larger deformations than any other record. There is no obvious

trend correlating lateral deformation with variation in material properties. Residual deformations are less than the transient deformations for both hazards at most elevations.

The phenomenon of frictional sliding is complex, and the behavior may vary throughout the monument depending on material characteristics and workmanship. The models take into account surface roughness through the friction coefficient and shear capacity under tensile stress through the clamping elements. The effect of interlock is not taken into account directly. As such, these analyses may over-predict lateral sliding deformations. The essential conclusion is that all permutations of the model under both the Mineral and MCE hazards result in deformations that are small relative to the size of the monument, and the performance is stable.

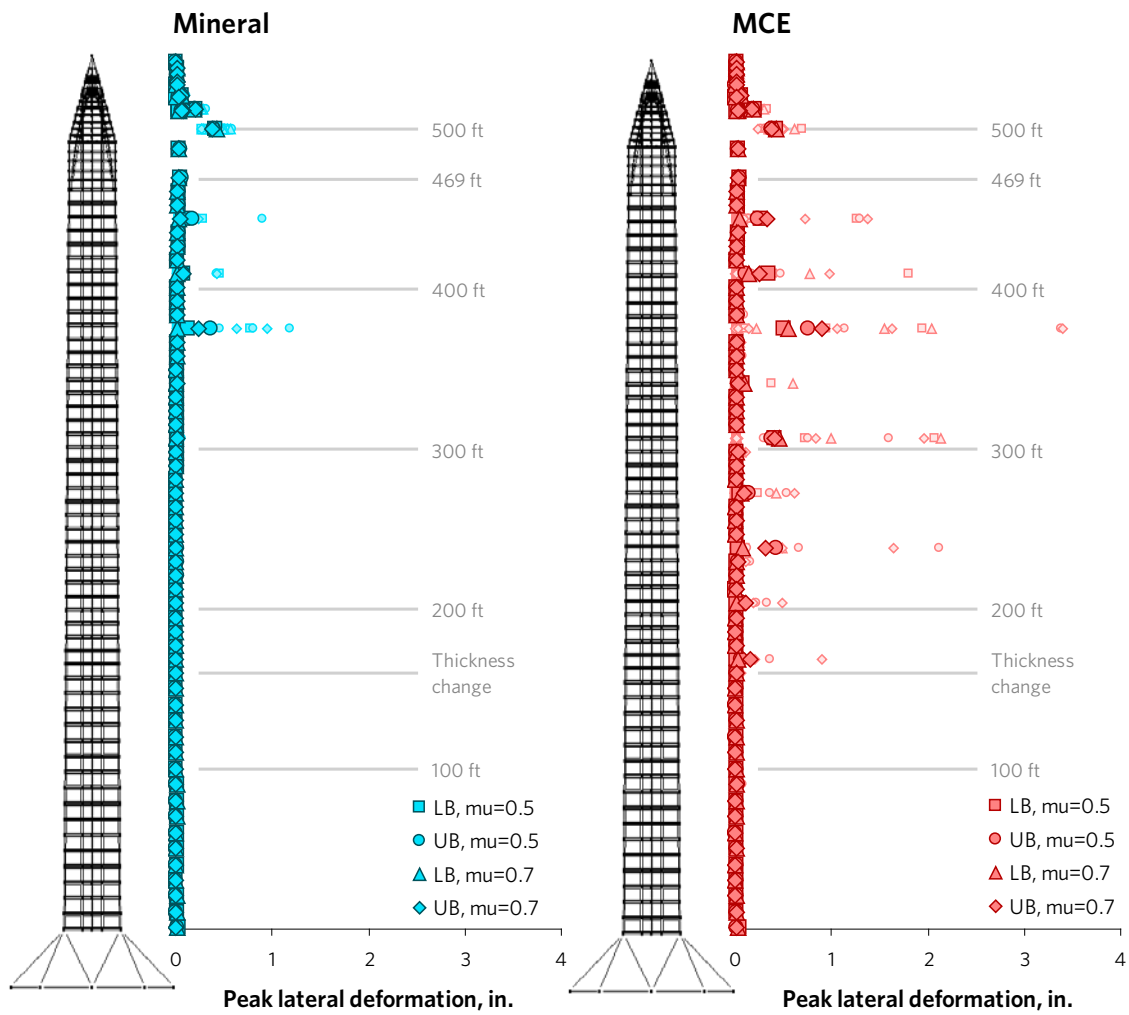


Figure 13-3 Graphs of peak transient lateral deformation results from slider elements: left, for the Mineral hazard; right, for the MCE hazard. The larger, darker markers indicate the mean response; shaded markers show results for individual records.

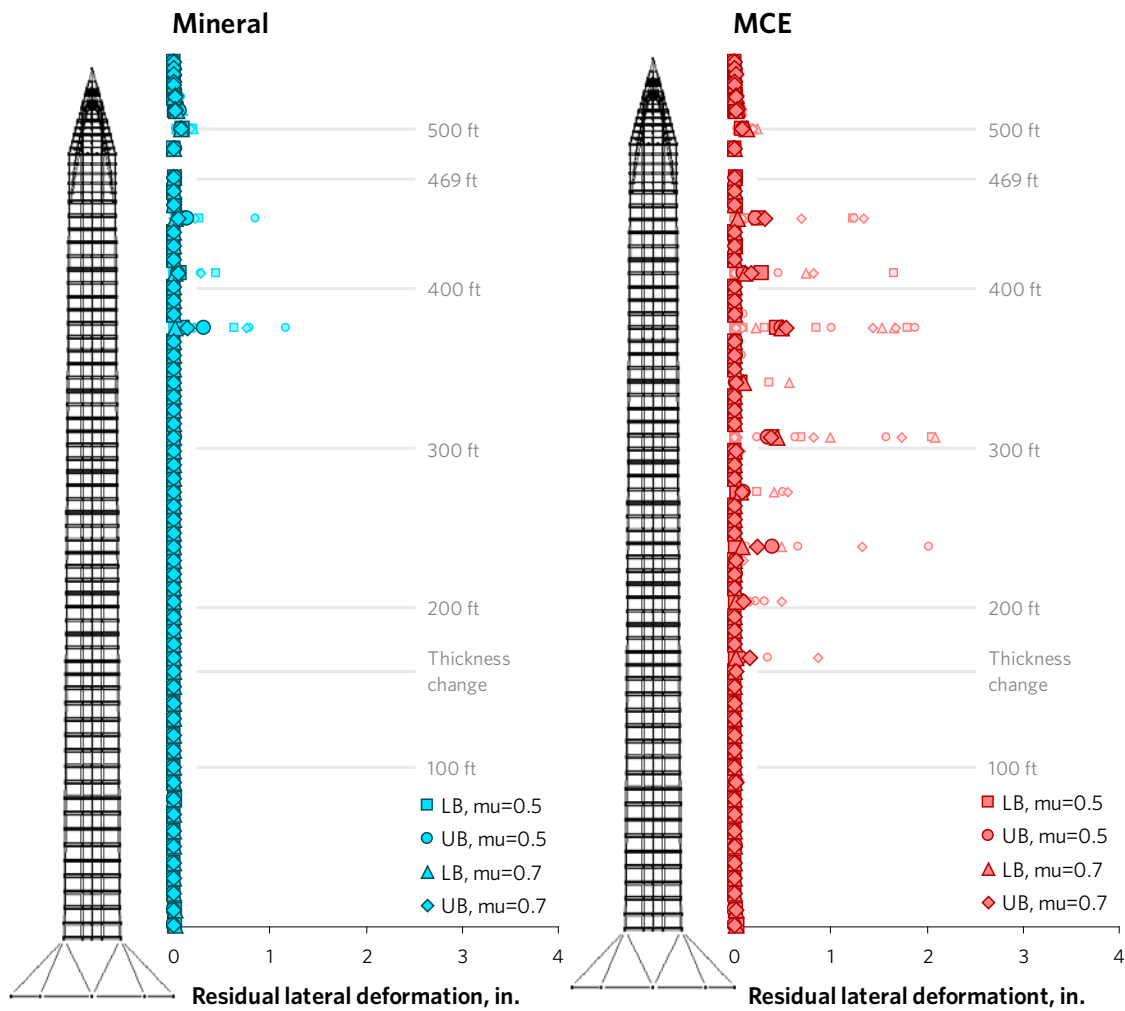


Figure 13-4 Graphs of residual lateral deformation results from slider elements: left, for the Mineral hazard; right, for the MCE hazard. The larger, darker markers indicate the mean response; shaded markers show results for individual records.

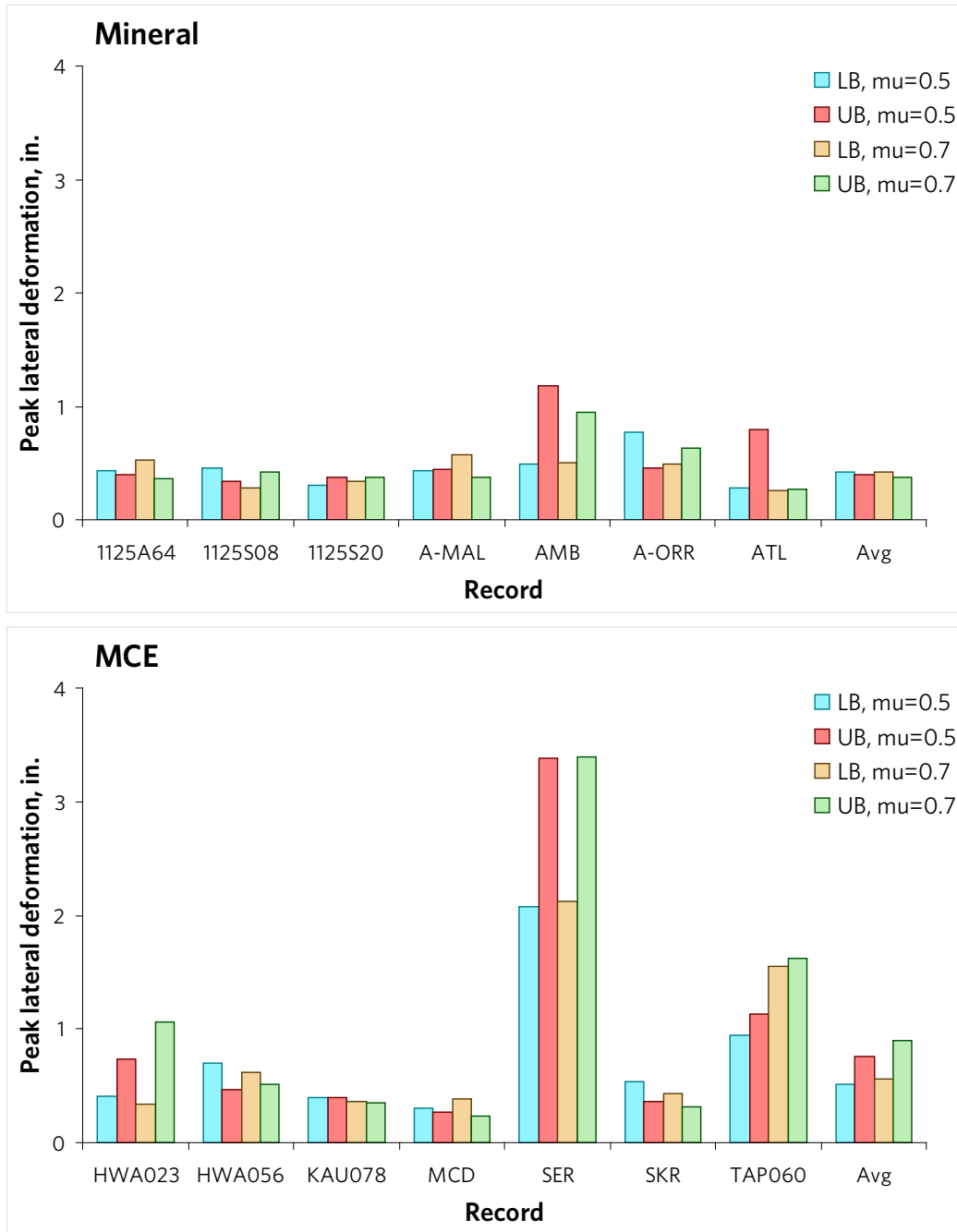


Figure 13-5 Graphs enveloping peak transient lateral deformation results in the slider elements: above, for the Mineral hazard and below, for the MCE hazard. Values are the maximum deformation occurring during each record.

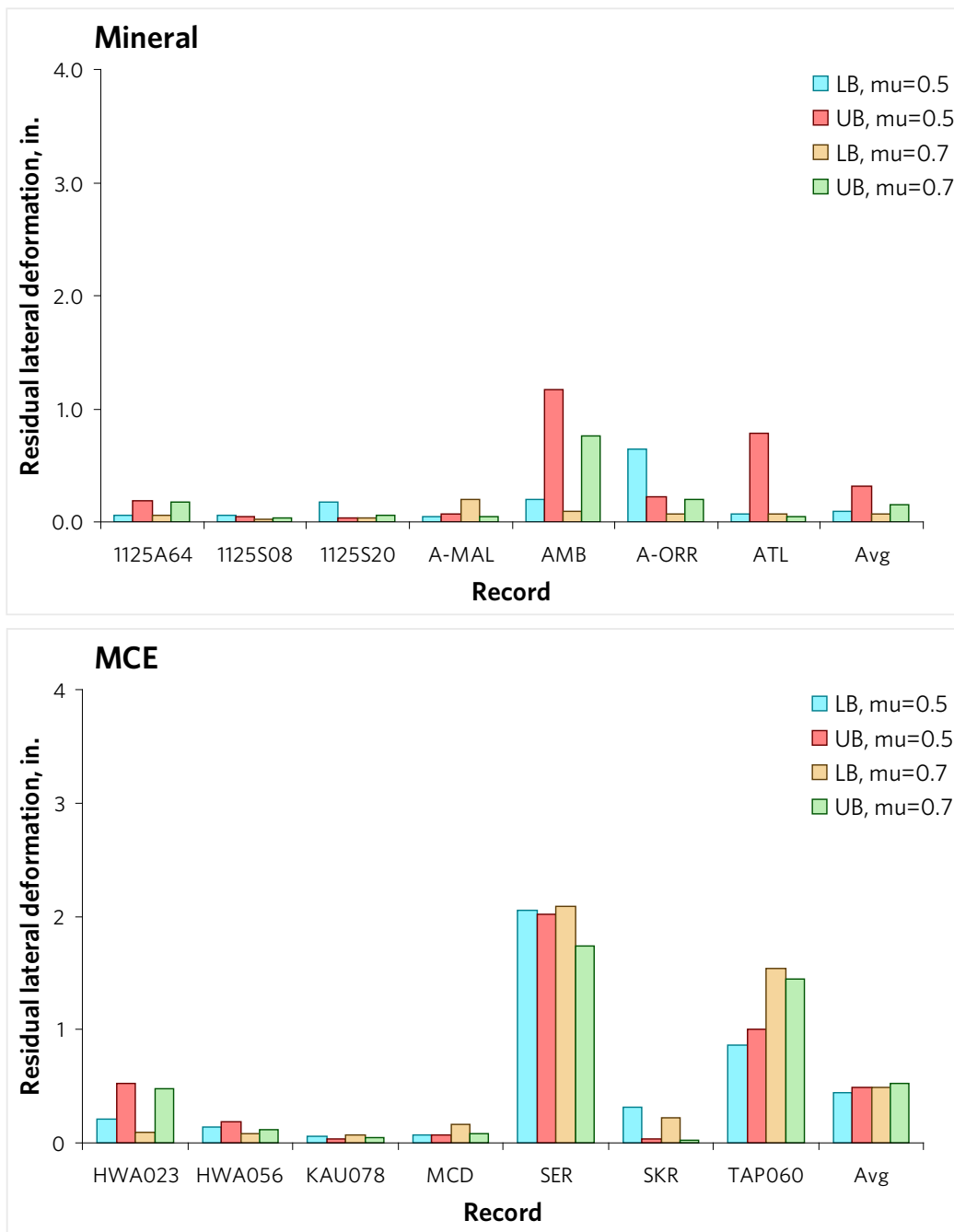


Figure 13-6 Summary graphs of residual lateral deformation results in the slider elements: above, for the Mineral hazard and below, for the MCE hazard. Values are the maximum deformations occurring during each record.

### 13.4 Widening of horizontal joints

The slider and wall elements are modeled to allow vertical deformations to occur across the elements; i.e. they can potentially crack. This deformation is tracked and interpreted as an estimate of the size of

horizontal widening of horizontal joints that may occur during an earthquake. Peak transient results are summarized in Figure 13-7 for all four permutations of the model and for both hazards. Residual deformations are plotted in Figure 13-8.

The deformations are negligible for the Mineral hazard below the pyramidion. Above that, there are small deformations ranging between nearly zero and about 0.2 inches. The average peak crack size for the Mineral hazard in the pyramidion is about 0.1 inches.

Similar results shown for the MCE hazard indicate minor cracking occurring in the monument below the pyramidion. On average, the cracking is less than 0.05 inches (about 1/16 inch). There appears to be a correlation in the MCE results in which the locations of significant lateral deformations illustrated in Figure 13-3 (right) correspond to locations of significant cracking illustrated in Figure 13-7 (right). However, the vertical deformations are comparatively larger in the pyramidion whereas the lateral deformations are larger in the tower. This illustrates a mode of behavior in which the pyramidion tends to rock slightly on the ribs and to slide less. This compares with the behavior of the lower part of the tower which slides more but lifts very little.

Residual vertical deformations are small for both hazards and for all four permutations of the model as illustrated in Figure 13-8. This implies that any significant horizontal cracks opened during an earthquake are likely to close again due to gravity effects once the shaking ends.

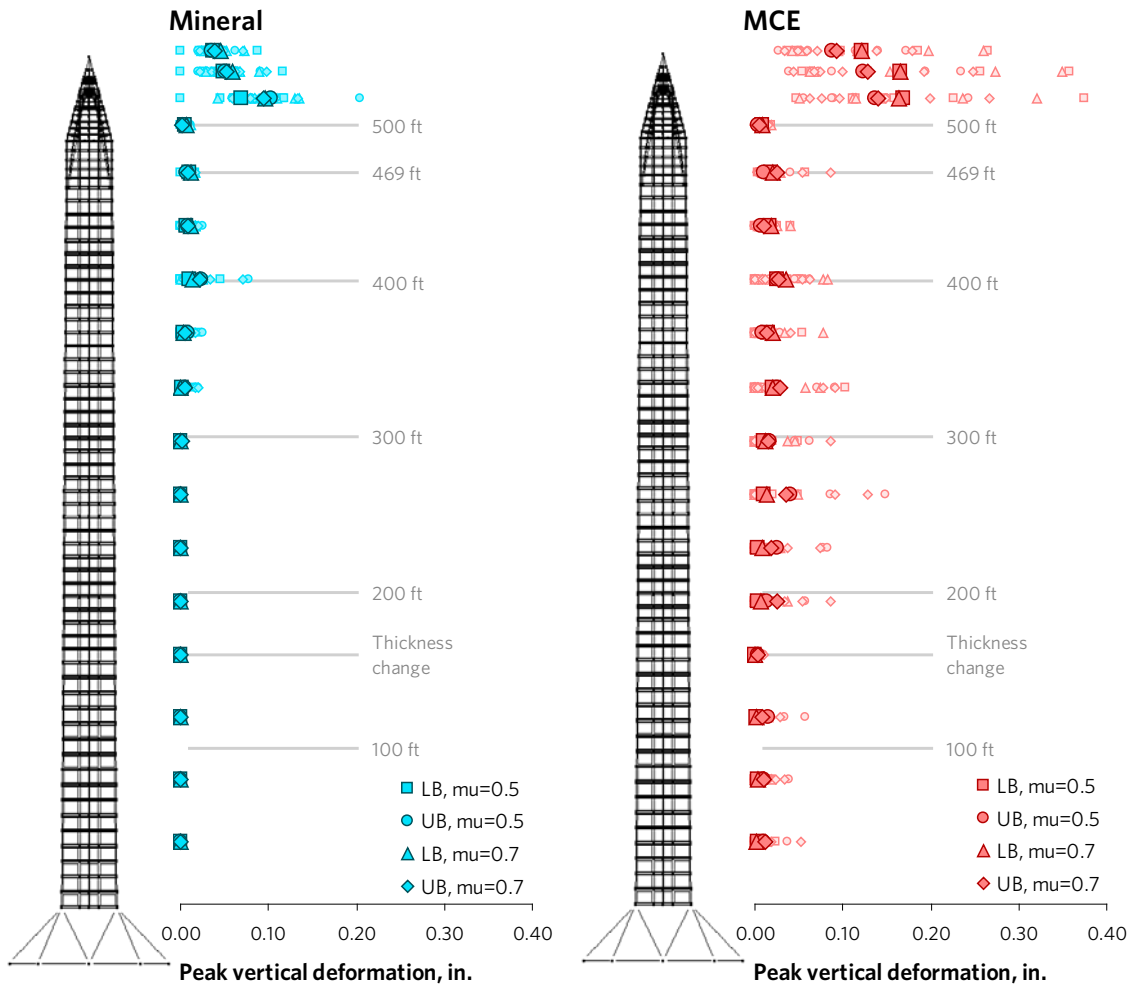


Figure 13-7 Graphs of estimated peak transient horizontal crack widths: left, for the Mineral hazard and right, for the MCE hazard. The values are the peak vertical tensile movement occurring at the slider elements. Shaded small dots show individual records; larger dots indicate the mean of the seven records.

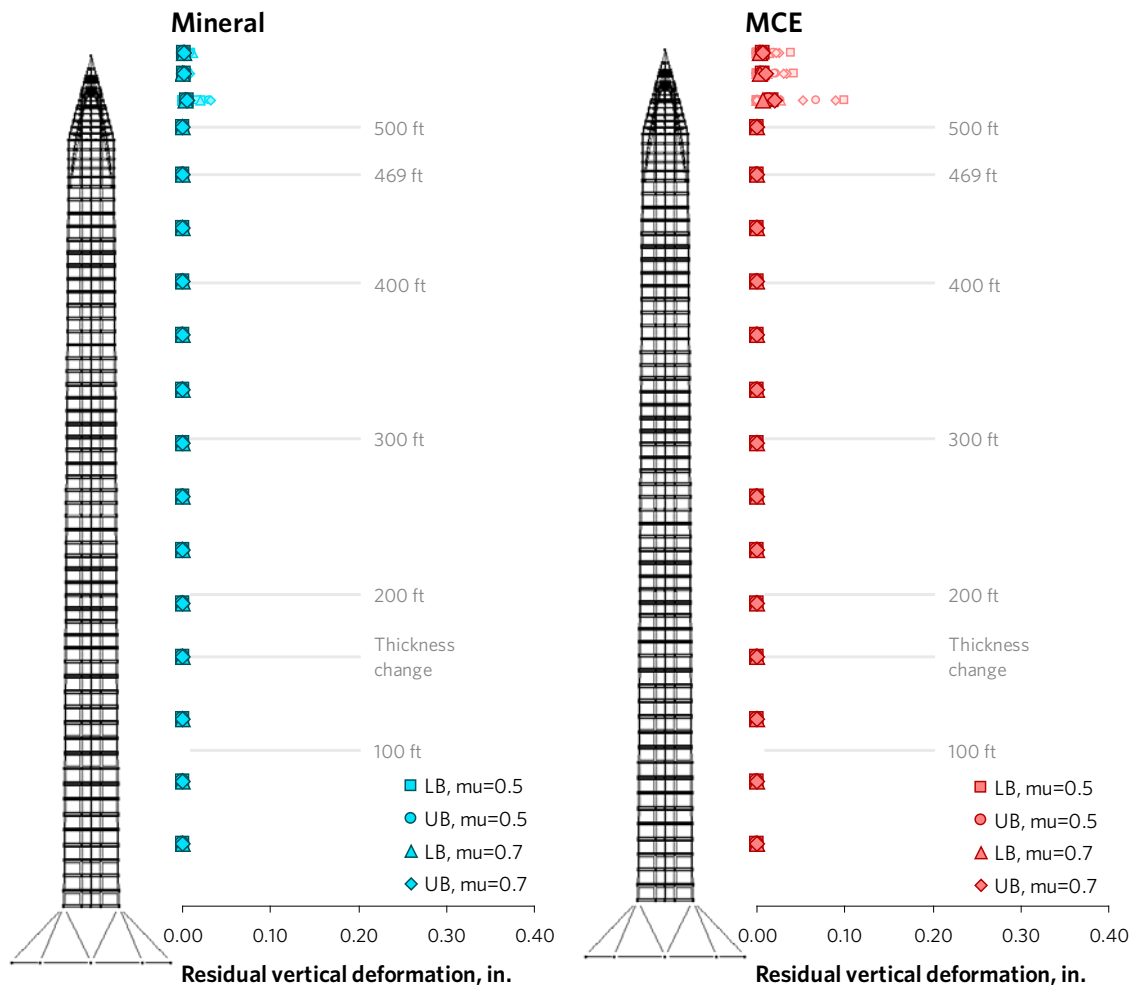


Figure 13-8 Graphs of estimated residual horizontal crack widths: left, for the Mineral hazard and right, for the MCE hazard. The values are the residual vertical tensile deformation after the shaking has ended. Shaded small dots show individual records; larger dots indicate the mean of the seven records.

### 13.5 Widening of vertical joints

The wall elements comprise fibers that lose strength in tension according to the masonry material model. As illustrated in Figure 8-1, tensile capacity in the horizontal direction is necessary to equilibrate lateral forces and bending moments that occur during an earthquake. If this tensile capacity is exceeded, an analytical crack occurs within the element. In the context of the monument, this would represent an action in which the joints among stones in the same course are enlarged. Figure 13-9 illustrates locations where such widening of the joints may occur. Eight representations of the model are shown representing the four permutations of the model analyzed under the two seismic hazards. The wall elements are colored to indicate locations of spreading of vertical joints (i.e. locations of significant tensile strain in the wall elements in the horizontal direction). The values are the mean of

the seven records analyzed. The colors are selected so that red elements would have 0.4 inches of cracking over a 40-foot wide zone (i.e. 0.1 inches of cracking over a 10-foot wide zone).

All permutations of the model show horizontal tensile strains in the pyramidion panels greater than 0.1 inches per 10 feet. The largest tensile strains below the 470-foot elevation occur under the MCE hazard for the two models with lower bound assumption of masonry stiffness. The tensile strains are largest at the base of the monument where the tower walls comprise the rubble/stone composite and extend to near mid-height of the tower. A similar pattern appears under the Mineral hazard for the lower bound assumption of masonry stiffness, but to a lesser degree. The models with upper bound stiffness show no such tensile strain below the pyramidion.

The analysis indicates widening of joints near the base of the monument for the Mineral event, for permutations of the model with lower bound masonry properties on the order of about 0.2 inches over the width of the monument. No widening is indicated for the other permutations of the model. These deformations were not observed after the 2011 earthquake. There are a few possible explanations of this apparent discrepancy:

1. The analysis indicates no such widening of joints for the upper bound masonry properties. Therefore, perhaps the upper bound stone properties at the base represent more closely the properties of the monument in situ.
2. The predicted deformations are very small relative to the dimensions of the monument near the base. There are approximately twenty (20) vertical joints in each course of stone. If the 0.2 inches of total widening were distributed evenly, this would amount to 0.01 (1/100) inches of widening per joint. This small amount of deformation may be difficult to observe.
3. It is possible that some permutations of the model over-predict these deformations. This should be taken into account when extrapolating to predict behavior under the MCE. In general, the deformations are small as to be of little concern with respect to potential observable damage or stability.

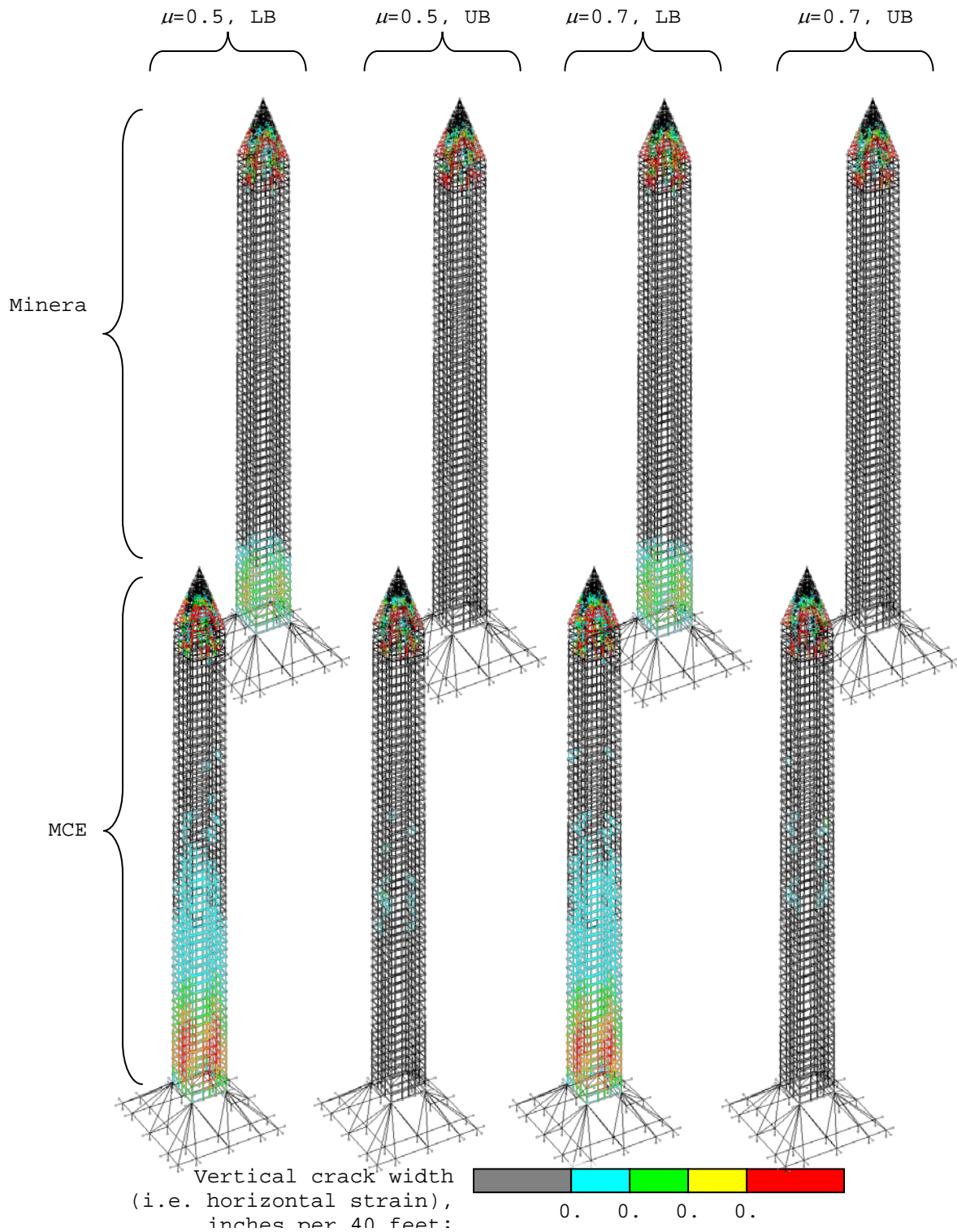


Figure 13-9 Illustration of predicted widening of vertical joints between stones in the same course. The values are the peak transient values, taking the mean of the seven records.

### 13.6 Soil response

Peak deflections from the soil spring elements are recovered for all the permutations of the model and for both hazards. The soil springs deflect about one inch under gravity loading. None of the records cause the foundation to uplift; i.e. the soil remains in compression (negative stress) throughout each record. Peak deflections due to earthquake loading are summarized in Table 13-1; values are the peak incremental deflections added to the deflections under gravity loading. Peak incremental soil deflections averaged over the seven records are very small: less than 1/16 inch for any record. As discussed in section 4.2, the soil material in the model defines peak strength of about 18 ksf at a deflection of 1.5 inches. Thus, the largest total soil deflection of 1.05 inches is less than the deflection at which the peak soil strength in the model would be reached (1.5 inches).

Table 13-1 Maximum earthquake soil deflections in inches. The soil deflects about one inch under gravity loading alone; the values below are in addition to that.

Stone strength/stiffness	Friction coefficient	Hazard			
		Mineral		MCE	
		Average	Maximum	Average	Maximum
Lower bound	0.5	0.01	0.02	0.02	0.03
Lower bound	0.7	0.01	0.02	0.02	0.03
Upper bound	0.5	0.02	0.02	0.02	0.04
Upper bound	0.7	0.02	0.02	0.02	0.04

Figure 13-10 shows hysteresis plots for the version of the model with upper bound stone properties and friction coefficient resulting from two records, one from each hazard. The selected soil spring is located at a corner of the footing and is thus expected to deflect the most. The graphs represent the instances of largest soil deflection; other records and soil springs would show deflections less than those plotted here. It illustrates the behavior of the soil springs relative to the backbone curve modeled. Under gravity loading, the soil is loaded beyond the elastic range; any increase in deflection will result in energy dissipation and perhaps permanent deformations. The graph illustrates how small the expected movement under earthquake loading is compared with the movement that has already occurred under gravity loading.

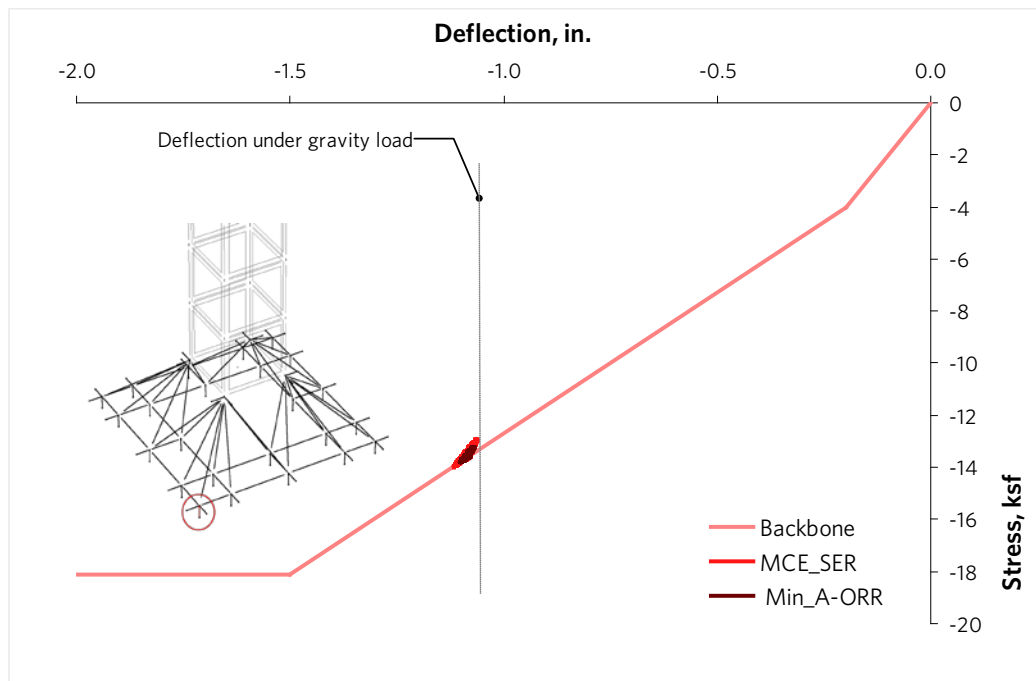


Figure 13-10 Graph of typical soil spring hysteresis (stress versus deflection). Positive values signify compression. The selected model has upper bound stone properties and friction coefficient. Results are from one MCE and one Mineral record.

## 13.7 Deformed shapes

In this section, images are shown from the model illustrating types of inelastic deformations that are evident in the response. The analysis indicates that potential inelastic deformations could occur in two general areas: in the pyramidion or in the mid-height of the tower (above the 250-foot level). In general the deformations in the monument are small relative to its size, much smaller than what would be expected for a conventional building. In order to illustrate the movement, the deformations in the following illustrations are scaled *significantly*.

### 13.7.1 Pyramidion

From the graphs in Figure 13-3, it appears that deformations in the pyramidion are likely for either the Mineral or MCE hazards. The largest average value of lateral sliding is around 0.4", depending on the permutation of the model under consideration. Figure 13-11 illustrates the type of deformation that is typical of many records in the pyramidion. It is a snapshot taken from the model with upper bound friction coefficient but lower bound stone properties during the Mineral record, A-ORR at 10.4 seconds. The image is a close-up of the pyramidion part of the model, with the face panels and secondary ribs removed to highlight the primary ribs. This particular record was selected to represent the response that might be typical of many other records. At the point in time when the snapshot was taken, the monument swayed mainly in a direction parallel to two sides, with some movement along the diagonal. The total tip displacement is about 3.6", or 0.06% of the height of the monument. There are lateral deformations occurring perpendicularly to one set of ribs that range from 0.4 inches at the base of the pyramidion to 0.14 inches near mid-height. In comparison with the ribs which are approximately 14

inches thick, these deformations are small. Nothing was observed during the analysis to indicate that the ribs may become unstable.

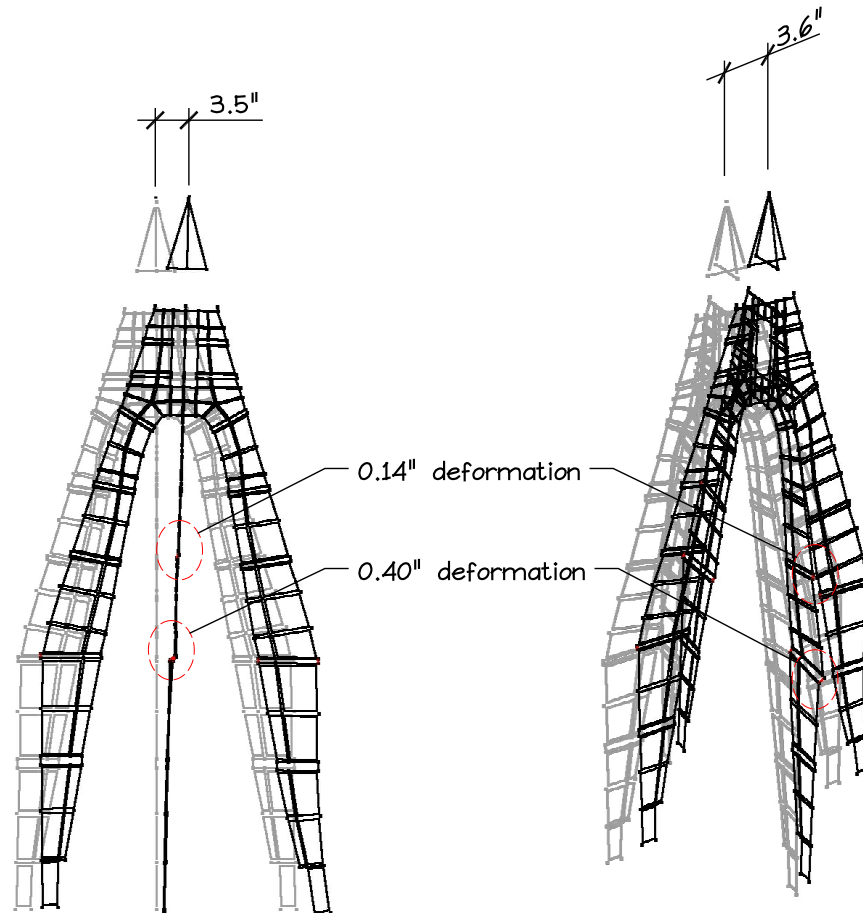


Figure 13-11 Snapshot of pyramidion taken from the Mineral A-ORR record at 10.4 seconds. The model shown assumes the upper bound friction coefficient but lower bound stone stiffness and strength properties. The face panels and secondary ribs are hidden to highlight the primary ribs. The deformations are scaled by a factor of 20.

### 13.7.2 Mid-height

The graphs in Figure 13-3 indicate potential for nonlinear deformations below the pyramidion for a number of MCE records. These results appear in all the versions of the model but are most pronounced for those with upper bound assumptions for stone stiffness and strength and mainly for the MCE hazard. Such deformations evident in the results of the Mineral analyses are comparatively minor.

Figure 13-12 illustrates the type of deformation that may occur. It is a snapshot taken from the model with lower bound friction coefficient and masonry properties during the MCE record, TAP at 56.2 seconds. The image shows a close-up of the model near the 375-foot level. This particular record was selected because the magnitude of the deformation is near the mean of the MCE records. At the point

in time when the snapshot was taken, the monument undergoes circular swaying in which the tip of the pyramidion moves around 10 inches in each direction, about 0.15% of the height of the monument. This movement is illustrated by the displacement time-history of the pyramidion tip shown in Figure 13-13. As the monument twists in this fashion, the tower experiences torsional moment along its axis. This torsional moment resolves into shear stresses and diagonal struts along the faces of the tower. Simultaneously, the swaying causes one corner of the monument to lift momentarily. Without reinforcement, the monument relies on friction in order to transfer shear stresses. The magnitude of available friction force is proportional to the bearing stress. As the corner lifts, the bearing stress reduces, and with that the ability to resist shear stress and torsional moment greatly diminishes, and sliding deformations result. After the monument twists, it becomes stable again and completes the analysis. There is no indication of instability during this movement.

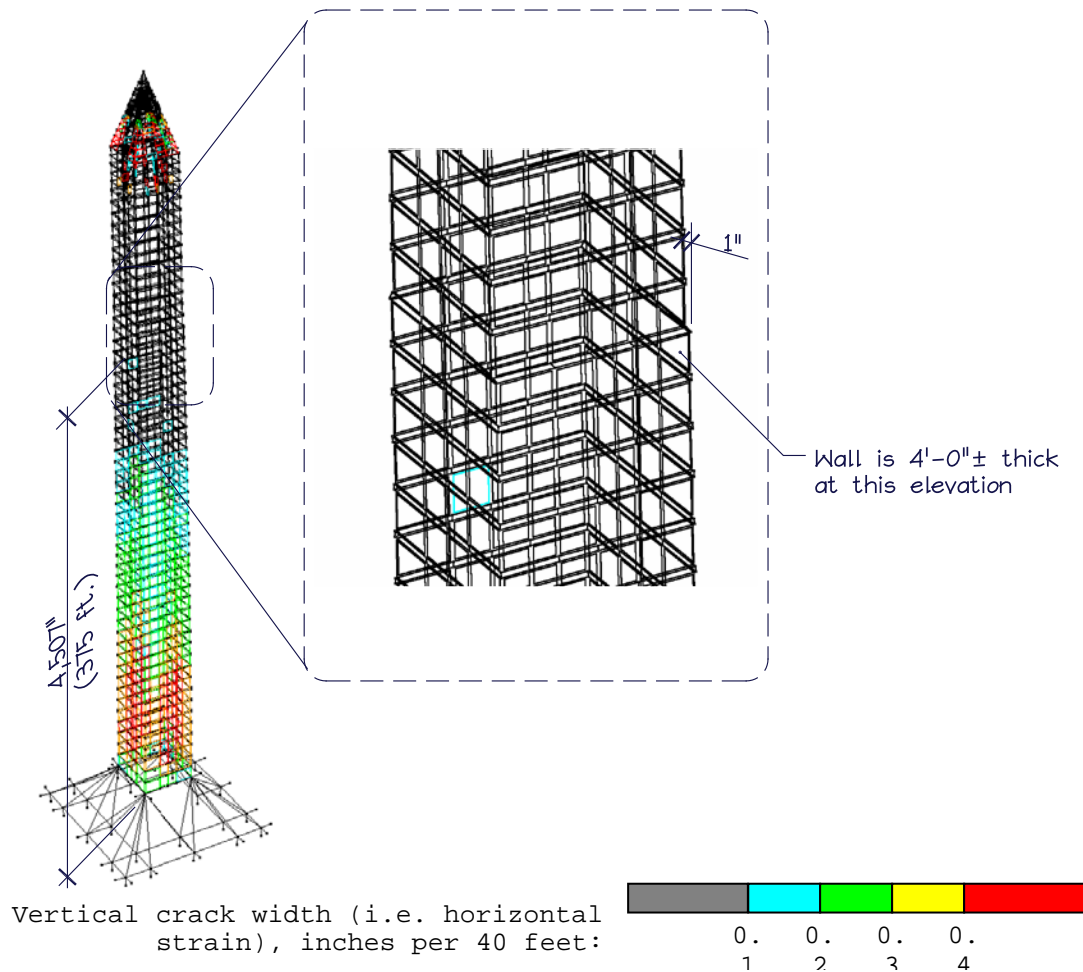


Figure 13-12 Snapshot taken from the MCE TAP record at 56.2 seconds. The model shown assumes the lower bound friction coefficient and masonry stiffness properties. The deformations are scaled by a factor of 10.

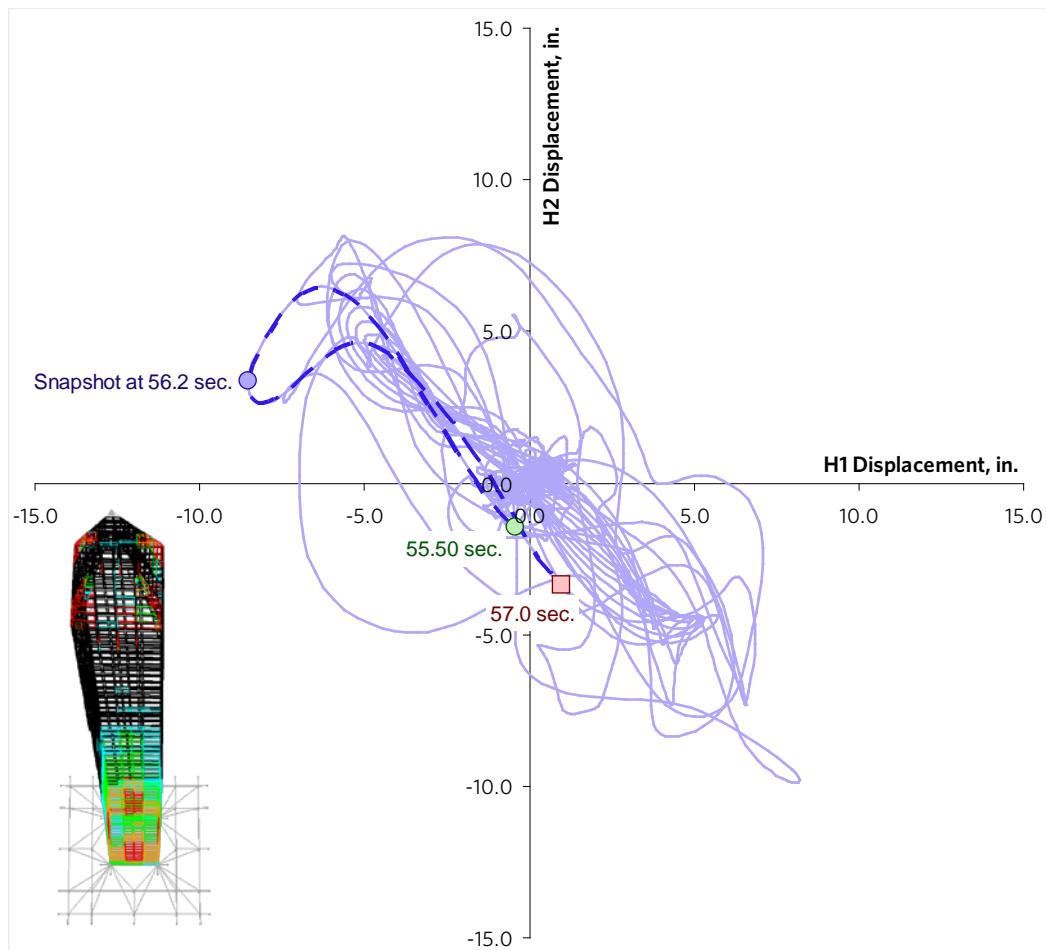


Figure 13-13 Graph of displacement time-history of top of monument from the MCE TAP record. The selected model assumes the lower bound friction coefficient and masonry stiffness properties. The image at the bottom left is a screen-shot from the model looking down with perspective. Deformations in the image are scaled by a factor of 10.

## 14 Bounding study: reduced tensile capacity

In the base models, the stone masonry is assumed to have an initial tensile capacity of 100 psi (refer to section 4.1); results of these analyses are reported in section 13. Section 14 reports selected results from another set of analyses in which the assumed initial tensile capacity was greatly reduced to 20 psi. Further, in these analyses the slider elements are allowed to slide under any amount of tensile stress in contrast to the base modeling in which sliding could only occur if the tensile stress exceeded 50 psi (refer to section 5.4). The intent of this study is to confirm that all possible modes of response that are taken into account despite the uncertainties around the mechanical properties of the stone masonry.

## **14.1 Lateral deformations**

Peak transient and residual lateral deformations were recovered from the friction slider elements. These results are analogous to what is reported for the base model in section 13.3. Figure 14-1 and Figure 14-2 show graphs of the peak transient and residual results, respectively. For both hazards, the largest transient and residual deformations occur just below the spring-line of the pyramidion ribs. The average deformations at the worst elevation are less than one-half inches for the Mineral hazard and less than one inch for the MCE. Peak transient deformations in the pyramidion are nearly equal for the two hazards at less than one-half inches on average. Residual deformations in the pyramidion are less than 0.3 inches for both hazards on average.

The graphs in Figure 14-1 and Figure 14-2 compare directly with base model results in Figure 13-3 and Figure 13-4. It is observed that the models with reduced tensile capacity show smaller peak and residual deformations at most elevations of the monument. The maximum deformations considering all elevations are similar in value but are less frequent in the model with reduced tensile capacity. The maximum deformations occur in different locations. The models with larger tensile capacity show several elevations at which the maximum deformation occurs, whereas those with reduced tensile capacity tend to show more of a concentration of deformations just below the spring-line of the pyramidion ribs.

The models with reduced tensile capacity general show smaller lateral deformations. However, these models show larger amounts of widening of vertical joints as described in the following section. There appears to be interplay between lateral sliding deformation and widening of vertical joints. In the base analyses, the lateral sliding deformations tended to be larger than the analyses with reduced tensile capacity, but the predicted widening of vertical joints tended to be less. This suggests that there may be a roughly constant amount of overall deformation that occurs under a given seismic hazard. The distribution of deformation varies among the mechanisms, depending on the modeling assumptions.

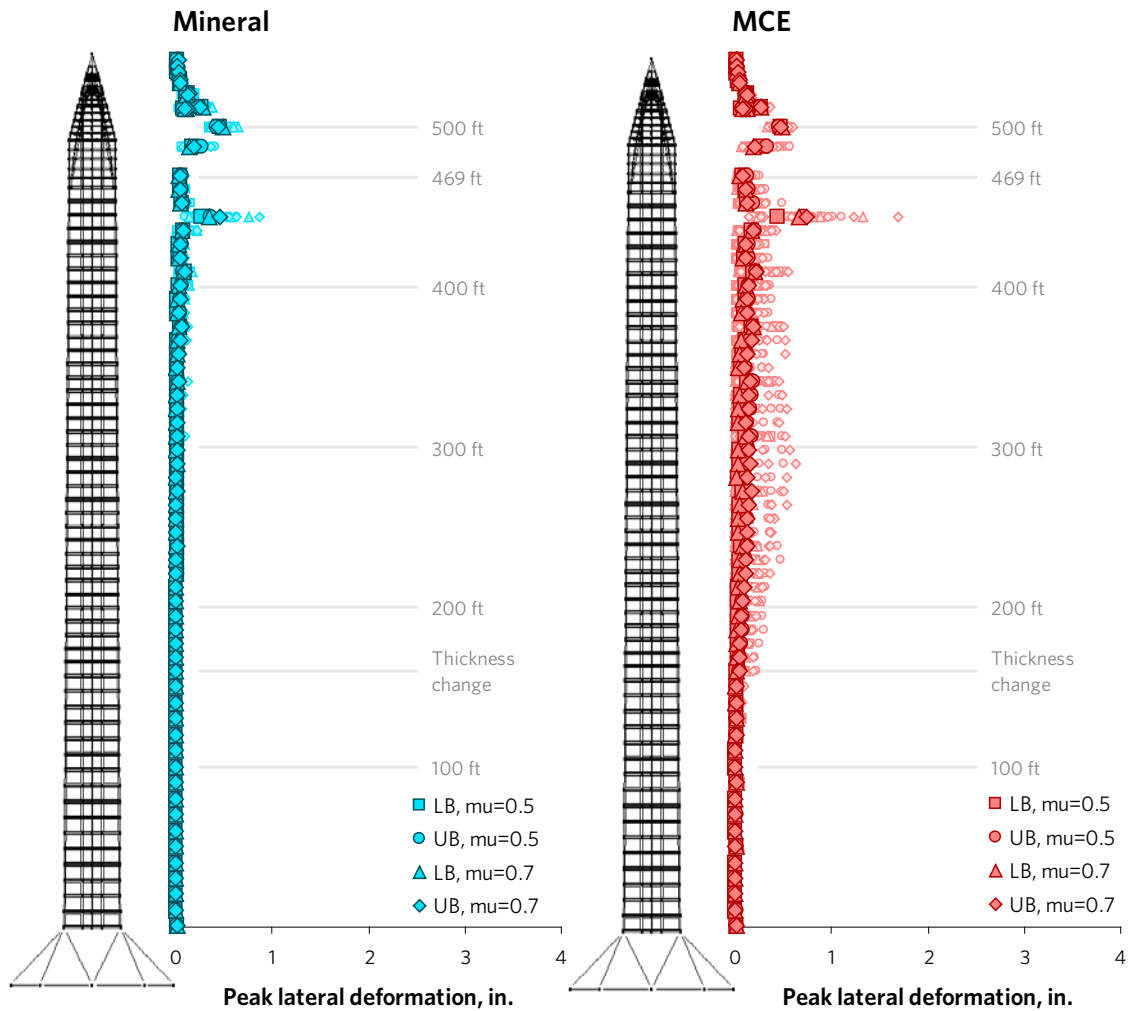


Figure 14-1 Results of bounding study with reduced tensile capacity. Graphs of peak transient lateral deformation results from slider elements: left, for the Mineral hazard; right, for the MCE hazard. The larger, darker markers indicate the mean response; shaded markers show results for individual records.

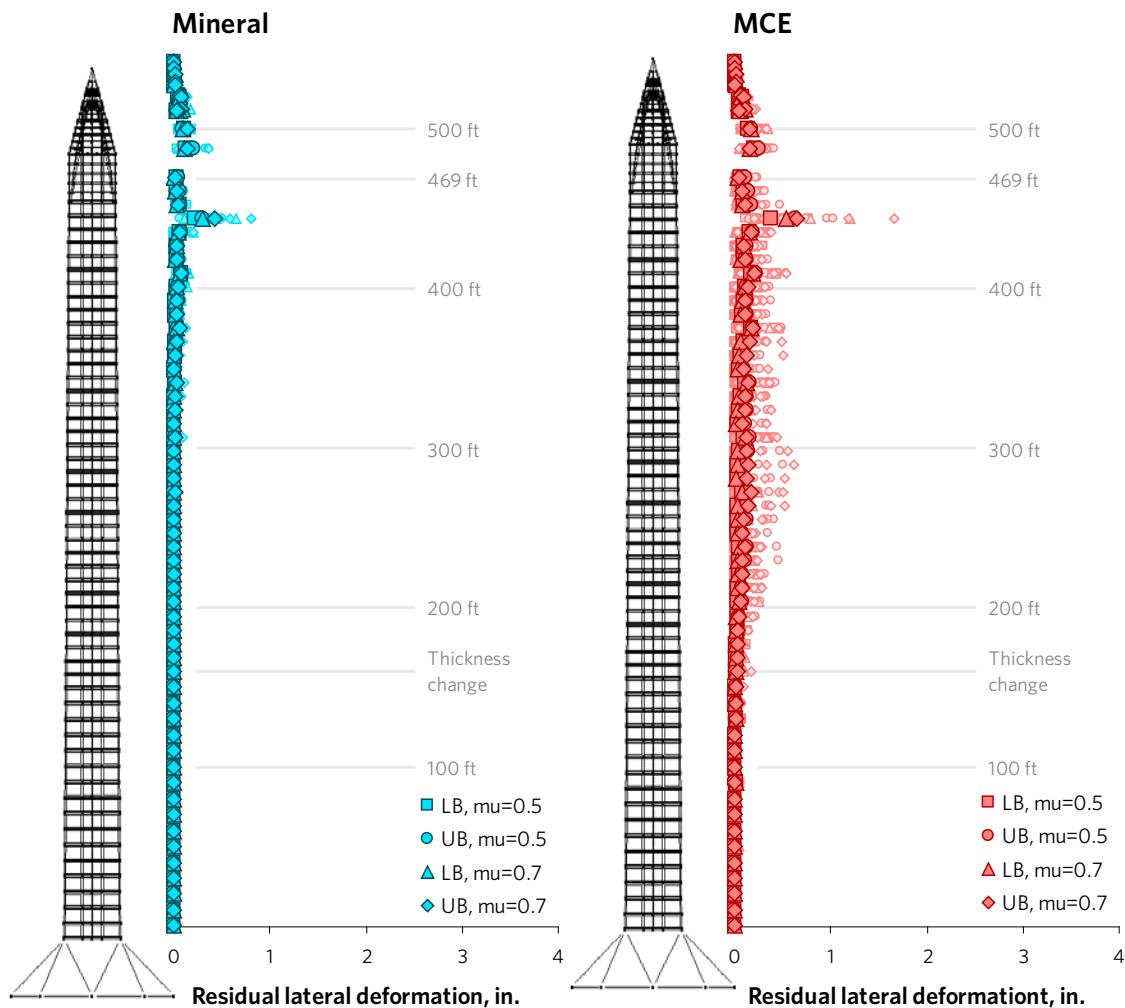


Figure 14-2 Results of bounding study with reduced tensile capacity. Graphs of residual lateral deformation results from slider elements: left, for the Mineral hazard; right, for the MCE hazard. The larger, darker markers indicate the mean response; shaded markers show results for individual records.

## 14.2 Widening of vertical joints

Figure 14-3 shows graphics from the model colored to indicate the magnitude of horizontal tensile strain in the wall elements, analogous to Figure 13-9 for the base model. Colored elements indicate locations in the monument in which the joints between stones in the same course would be expected to widen. Representations are shown of four permutations of the model (upper and lower bounds of masonry stiffness and friction coefficient) for each hazard, taking the average of the results from the seven records.

All permutations of the model show widening of joints in excess of 0.1 inches per 10 feet at some elevations. Generally, the Mineral hazard causes less of this deformation than the MCE, and models with upper bound masonry stiffness show less deformation than ones with lower bound stiffness. Friction coefficient appears to have a negligible effect on these results.

The results in Figure 14-3 are compared with the base model results in Figure 13-9. The model with reduced tensile capacity indicates larger and more frequent widening of joints in general. There is a similarity in that the models with lower bound masonry stiffness show horizontal tensile strains near 1 inch per 10 feet (red elements) in the lowest 160 feet of the monument. The models with reduced tensile strength show many more colored elements above 160 feet, and models with permutations of masonry stiffness show strains near 1 inch per 10 feet (red elements) near the 400-foot elevation.

Similarly to the base analyses, the analyses with reduced tensile capacity indicate widening of joints near the base of the monument for the Mineral event, for permutations of the model with lower bound masonry properties on the order of about 0.2 inches over the width of the monument. Possible explanations of this apparent discrepancy are noted in section 13.5, and apply here also.

In contrast with the base analyses, the analyses with reduced tensile capacity also indicate widening of joints in the upper part of the monument. Some such deformations were observed after the 2011 earthquake as noted in the *Post-Earthquake Assessment* by WJE (October 2011) and in the repair drawings by WJE, dated April 4, 2012. There were many existing vertical cracks and gaps between joints before the 2011 earthquake occurred, and the earthquake caused some additional damage, including new cracks, widening of joints and re-opening previously repaired cracks.

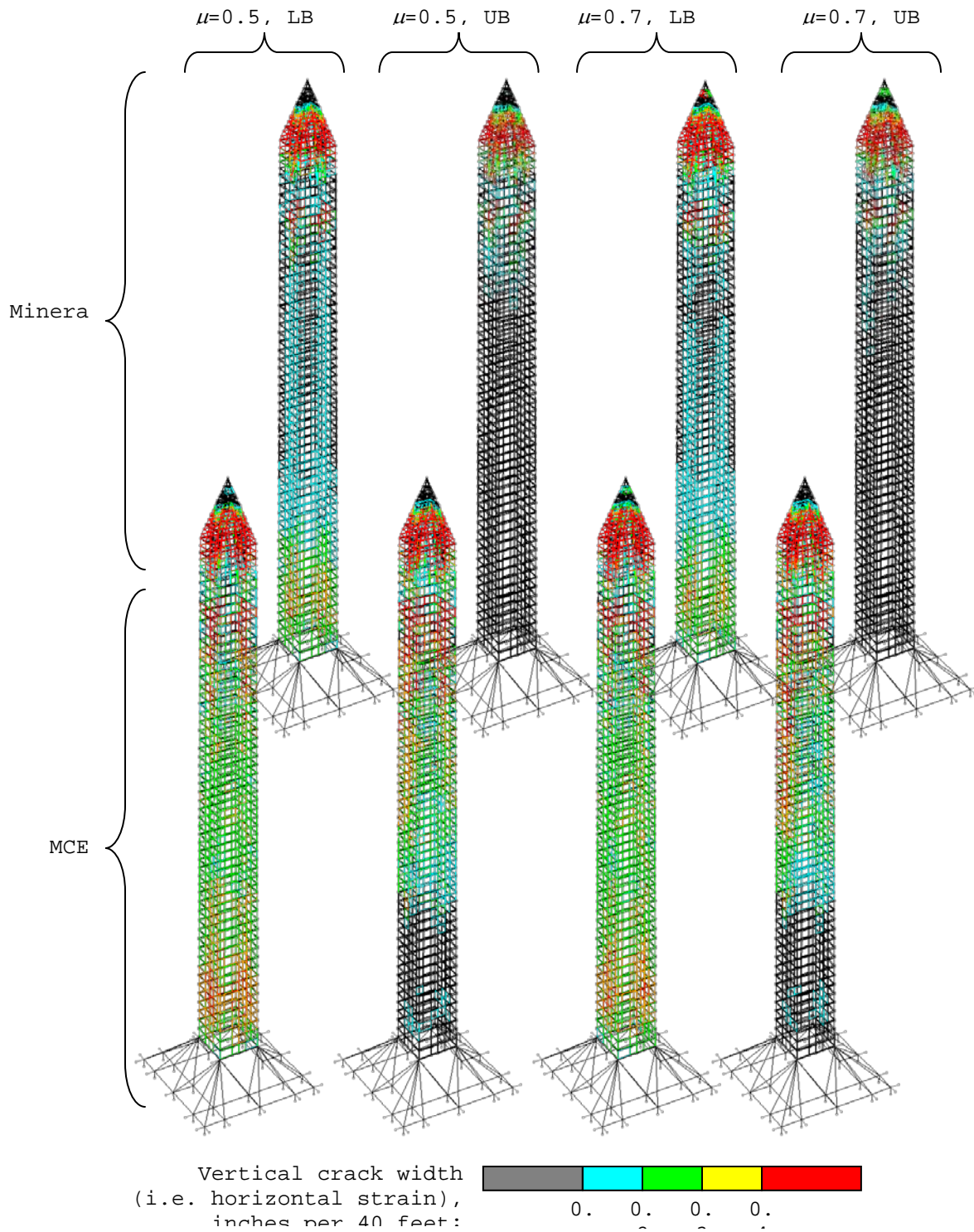


Figure 14-3 Results of bounding study with reduced tensile capacity. Illustration of predicted widening of vertical joints between stones in the same course. The values are the peak transient values, taking the mean of the seven records.

## 15 Conclusions and findings

This study supplements the seismic assessment performed by *Wiss, Janney, Elstner Associates, Inc. (WJE)*. The results of the analysis have corroborated the results and recommendations found in the *WJE* report, and in the case of the Mineral earthquake, correspond to the observed damage. Detailed recommendations can be found in the *WJE* report.

In this section, the results reported in detail in the previous section are considered to synthesize conclusions and support recommendations. A model was built to emulate the nonlinear dynamic behavior of the monument. It may not be appropriate for predictions about the precise magnitude and specific locations where damage might occur. There are areas of significant uncertainty in regard to the properties of the stone: friction coefficient, stiffness, and strength. To address these uncertainties four versions of the model were analyzed, each one considering a different combination of friction coefficient and stone stiffness/strength to bound the potential structural response.

Two seismic hazards were considered, one representing what occurred at the monument during the earthquake that originated near Mineral, Virginia in August, 2011 and another representing the Maximum Considered Earthquake (MCE), provided by the geotechnical engineer, *AMEC Environment & Infrastructure*. The spectral accelerations of these hazards are similar up to a period of about 0.6 seconds and both have peak spectral acceleration of about 0.3g at a period near 0.3 seconds. For periods larger than 0.6 seconds, the spectra diverge, and the MCE is significantly larger.

The displacement response of the monument is small relative to its height compared with other conventional structures considering large shaking. Displacements under the MCE are generally larger than those under the Mineral hazard, but the largest displacement result from any record is 0.3% of the height of the monument, or about 16.7 inches. Most of this displacement is accommodated by the monument elastically with limited nonlinear response. The acceleration response of the structure is on the order of 0.8g for both the MCE and Mineral hazards.

Many records, under both the Mineral and MCE hazards, result in nonlinear lateral deformations in the pyramidion. These deformations are on average less than 0.5 inches. After the Mineral, Virginia earthquake that occurred in 2011, it was observed that some shifting did occur in the ribs of the pyramidion, in one case about 0.25 inches. Given that the ribs are about 14 inches thick, these displacements are relatively small and would not give rise to concerns over the stability of the ribs. Under the standard framework for seismic evaluation per ASCE 41-06 in which the average response from the set of seven records is considered relative to the risk of collapse, retrofitting the ribs to improve stability is not warranted.

Under the MCE in the base analyses, nonlinear lateral deformations occur below the pyramidion above the 200-foot level. In cases where this does occur, the peak transient and residual deformations are less than one inch on average. This deformation is characterized as a twisting deformation rather than a lateral offset of the entire tower. In the analyses in which the tensile capacity of the masonry was greatly reduced, the frequency of the locations where these deformations occurred was reduced, yet the maximum deformation remained roughly the same. There is no indication that this sort of damage represents a collapse or life safety hazard. Under the standard framework for seismic evaluation per

ASCE 41-06 in which the average response from the set of seven records is considered relative to the risk of collapse, retrofitting the tower to prevent this behavior is not warranted.

During shaking under both hazards, some transient widening of horizontal joints is evident in the analysis. It is generally largest in the pyramidion for the Mineral hazard where it ranges between 0.1 inches and 0.5 inches. In the MCE analyses it also occurs lower down in the monument but is of a smaller magnitude, ranging between 0.1 inches and 0.2 inches. These cracks are predicted to close once the earthquake ends.

During shaking under both hazards, some widening of the vertical joints between stones in the same course is evident. In the base model analyses the widening is greatest for the permutations of the model with the lower bound assumption for stone stiffness, occurring mainly near the base for the MCE hazard where it is on the order of 0.1 inches per 10 feet. In the Mineral analyses it also occurs, but to a lesser degree. In the analyses in which the tensile capacity of the stone is greatly reduced, there is an increase in the frequency of locations at which these deformations are predicted, but not a significant increase in the magnitude of widening. The amount of widening indicated by the analyses is small relative to the thickness of the walls and do not appear to pose a collapse nor life-safety hazard.

The soil under the monument is modeled based on recommendations from the geotechnical engineer, AMEC. Under both the Mineral and MCE hazards, incremental settlement due to shaking is expected to be negligible.

The response of the eight permutations of the model (varying masonry stiffness, compressive and tensile strength, and friction coefficient) taken together represent a range of potential behavior of the monument. Some permutations indicate deformations similar to those observed after the Mineral earthquake in 2011. All of permutations result in deformations that are minor with respect to the size of the structure. Furthermore, all permutations show stable response to both the Mineral and MCE hazards.

## **16 Recommendations**

Plans for repairing damage to the panels in the pyramidion resulting from the Mineral earthquake have been developed by *Wiss, Janney, Elstner Associates, Inc. (WJE)*. We would recommend extending the scope of construction beyond repairing the evident damage to include similar areas of the pyramidion that may be damaged in future earthquakes. In particular, it may be feasible to use the same type of brackets that are shown in the repair plans to provide a positive connection between the more vulnerable panels and supporting ribs. This connection would be for the purpose of reducing the potential falling hazard from panels in the event of a future strong earthquake. We understand from *WJE's* detailed damage survey that nearly all of the damaged connections, and all of the severely damaged connections, were at locations where two panels were supported by a rib and that very few single-panel connections were damaged. This demonstrates that the two-panel connections are more likely to introduce potential falling hazards during future strong earthquakes and that these connections are the better candidates for retrofitting.